RSC Advances

ROYAL SOCIETY OF CHEMISTRY

www.rsc.org/advances

Experimental and theoretical study on thermal decomposition of methyl butanoate behind reflected shock waves

A. Parandaman, M. Balaganesh, and B. Rajakumar*

Department of chemistry, Indian Institute of Technology Madras, Chennai-600036, India.

*Address for correspondence: rajakumar@iitm.ac.in

Abstract

Thermal decomposition of methyl butanoate (MB) diluted in argon was studied behind the reflected shock waves in the temperature range of 1229-1427 K using single pulse shock tube (SPST). The post shock mixtures were analyzed quantitatively using gas chromatography (GC) and qualitatively using Fourier-transform infrared (FTIR) spectroscopy. Methane (CH_4), ethylene (C_2H_4), and acetylene (C_2H_2) were the major decomposition products. The minor products are ethane (C_2H_6), propylene (C_3H_6), 1,3-butadiene (C_4H_6) and methyl acrylate ($C_4H_6O_2$). The obtained first order rate coefficient for the decomposition of MB is k_{total} (1229-1427 K) = (3.08 ± 1.11) × 10^{12} exp (-(53.6 kcal mol^{-1} ± 4.7)/RT) s^{-1}, and for the formation of C_2H_4 channel, the rate coefficient obtained to be $k_{ethylene}$ (1229-1427 K) = (7.92 ± 2.72) × 10^{9} exp (-(47.6 kcal mol^{-1} ± 4.5)/RT) s^{-1}. Theoretical kinetic calculations were also performed for the unimolecular hydrogen transfer reactions using canonical variational transition state theory (CVT) with small-curvature tunneling (SCT) corrections. The temperature dependent rate coefficients for the overall reaction were computed in the temperature range of 500-2500 K, and were used to derive the Arrhenius expression: k_{total}^{theory}(500-2500 K) = (9.05 ± 1.91) × 10^{13} exp (-(70.7 kcal mol^{-1} ± 2.0)/RT) s^{-1}. A reaction scheme containing 39 species and 66 elementary

reactions was proposed to simulate the reactant and product concentrations over the temperature range of 1229-1427 K. The agreement between the experimental results and the model prediction for all the species is observed to be good. The decomposition of MB happens mostly via intramolecular hydrogen transfer than C-C bond and C-O bond fission. Majority of these intramolecular hydrogen transfer reactions are lower energy barrier reactions than the homolytic bond fission reactions.

Keywords: methyl butanoate; single pulse shock tube; canonical variational transition state theory

1. Introduction

Solid, liquid, or gaseous biofuels are derived from renewable biological sources. Biomass can be converted to high value energy sources including ethanol, biodiesel, methanol, hydrogen, or methane.[1,2] They are considered as alternative fuels for the transport sector and are expected to reduce our dependence on petroleum. In addition, biofuels minimize the effects on climate because they produce fewer greenhouse gases than gasoline or diesel.[3,4] Biodiesel is the mostly used biofuel. Typical biodiesel consists of mixtures of saturated and unsaturated methyl esters containing carbon chains with 16 or more atoms in length that are generally derived from animal fats and vegetable oils[5,6] (soybean oil in U.S. and rapeseed oil in Europe). Although methyl butanoate (MB) do not have larger molecular weight like a typical biodiesel, it has the essential chemical structural features, namely the R-(C=O)-O-CH_3 structure (where R is an alkyl group). Hence, the resultant reaction mechanism is smaller and will be of more manageable size than that of a larger hydrocarbon.[7] The reaction rate coefficients for larger methyl esters are primarily based on the kinetic parameters of smaller methyl esters (e.g., methyl butanoate).[8,9] Therefore, accurate knowledge of the kinetic parameters for such smaller methyl esters is essential in the development of the detailed mechanism of biodiesels for practical purposes.

The combustion chemistry of lower methyl esters has gained a focus of attention for the past one and half decade.[10] MB has been chosen as a surrogate for biodiesel fuels, and various theoretical and experimental studies on this molecule have been reported in the literature.[11-14] Fisher *et al.*[15] developed the first complete chemical kinetic mechanisms for the oxidation of methyl formate and MB. However, they have validated their mechanism with the available experimental data in temperature range of 550-675 K. Hakka *et al.*[16] developed detailed chemical kinetic mechanism for the oxidation of MB, based on their shock tube and a jet-stirred reactor

experimental data. Similarly, Dooley *et al.*[17] developed a detailed mechanism for the oxidation of MB and it was tested with their shock tube and rapid compression reactor data. They have reported the ignition delay times as well. A review by Lai *et al.*[18] summarizes the research to date on biodiesel molecules, including MB. Recently Ali and Violi[19] studied unimolecular decomposition pathways (C-C, C-O bond fissions and hydrogen migrations) of MB and the corresponding rate constants, using ab initio methods in combination with transition state theory. In addition, the rate coefficients for the unimolecular elimination channels were computed using the master equation approach, in their studies. Overall, various studies on MB pyrolysis and oxidation were carried out with appropriate kinetic mechanisms. However, most of these studies have paid attention only on oxidation of MB.

In the present investigation, thermal decomposition of MB was studied experimentally for the first time in the temperature range of 1229 - 1427 K behind the reflected shock waves. The complete degradation products were followed and appropriate mechanism for the decomposition is suggested in this study. In order to further understand the experimental measurements, we also report the rate coefficients for hydrogen transfer reactions in thermal decomposition of MB using canonical variational transition state theory (CVT) coupled with the hybrid meta density functional M06-2X with 6-31+G(d,p) basis set in broad temperature range of 500-2500 K. This study provides a complete picture of the major decomposition pathways of MB and the results can be used to improve the accuracy and completeness of the MB kinetic mechanism.

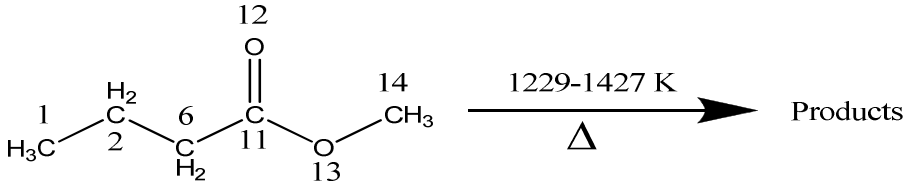

methyl butanoate

2. Experimental

The thermal decomposition of MB was studied behind the reflected shock waves in a 50.8 mm i.d. single pulse shock tube (SPST). The driver and driven section lengths are 1290 mm and 3440 mm respectively. The details of the experimental setup used in this work have been given elsewhere.[20] A 10 liter dump tank was connected to the driven section at 45° angle near the diaphragm station in order to prevent reflection of transmitted shock waves. The driver section was separated from the driven section by an aluminum diaphragm of various thicknesses depending upon the desired shock strength. Three pressure transducers are mounted towards the end of the driven section. The mounted pressure transducers were used to measure the shock velocity and thereby to calculate both the primary and reflected shock temperatures. The pressure transducer, which is mounted closest to the end flange, was used to record the pressure trace and reaction time, in the reaction zone. A typical pressure trace recorded using a piezoelectric pressure transducer mounted near the end of the driven section is shown in Figure 1. The arrival of both the primary and the reflected shock waves, and the reaction time are marked in the pressure trace. The constant voltage in the "reaction time" zone is the direct evidence for the nearly constant temperature condition in the carried out experiments. Shock velocities were calculated from the time taken for the shock wave to travel between the pressure transducers mounted on the driven section near the end of the shock tube. The reflected shock temperatures calculated by conventional Rankine-Hugoniot relations.[21]

The chemical thermometric method[22,23] was used in our investigations to get accurate reflected shock temperatures. Reflected shock temperatures were determined from the extent of decomposition of 1,1,1-trifluoroethane (CH_3CF_3) which was added in small quantities to the reaction mixtures to serve as an internal standard. It decomposes into $CH_2{=}CF_2$ + HF is a first

order unimolecular reaction, which has a rate coefficient[24] of k = 5.71 × 10^{46} $(T)^{-9.341}$exp (-47073 K/T) s^{-1}. The extent of decomposition of the internal standard in a given experiment, χ can be calculated using the below given equation

$$\chi = \frac{[Product]_t}{[Product]_t + [Internal\ standard]_t}$$

Where $[Product]_t$ is product concentration of internal standard at time '*t*' and $[Internal\ standard]_t$ is left out concentration of internal standard at time '*t*'

Using the calculated χ , the rate coefficient for the decomposition of the internal standard at the carried out experimental temperature and the reaction time is calculated using the below given relation

$$k_{int} = -\frac{1}{t} ln(1 - \chi)$$

The temperature behind the reflected shock wave can now be calculated using the temperature dependent rate coefficient equation for the unimolecular elimination of HF from 1,1,1-trifluoroethane reported by Akira *et al.*[24]

The reflected shock temperatures calculated using Mach number (T5-Ms) and internal standard method (1,1,1-trifluoroethane as internal standard) were observed to be differed by ~5-6 % in the studied temperature range. The temperatures calculated using shock speed are higher by ~5-6 %, which is acceptable given the errors in measurement of the speed of the shock, real gas effects and boundary layer effects. The use of chemical thermometric method eliminates most of the inherent uncertainties in the physical properties in these shock tube experiments as determined from the conservation equations. The introduction of the internal standard removes uncertainty in experiments because both the internal standard and target molecule experience the

same experimental conditions such as temperature, heating time and reaction pressures. Therefore, the temperatures measured using chemical thermometry method were chosen in our experiments and in subsequent analyses of the data.

The shock tube was pumped down to approximately 1×10^{-6} Torr for two to three times before the experimentation using a diffusion pump, after making the shock tube rich in argon environment. Reaction mixture containing 2% of MB and 0.2% of diluted CH_3CF_3 were prepared manometrically and diluted further with argon gas to a desired pressure. The reaction mixtures were loaded in the sample compartment of the shock tube, which is at the end of the driven section separated using a ball valve. While the sample compartment was filled with the sample and argon, the rest of the driven section was filled only with argon to a little higher pressure (about 10-15 Torr), to avoid the back diffusion of the sample when the ball valve is opened just before generating a shock wave. The shock waves were generated by rupturing a pre-scored aluminum diaphragm by loading desired pressure of ultra high pure helium in the driver section. After the experiment, the samples were directly transferred to the online six port gas sampling valve (having a constant volume loop of 0.5 ml) of the gas chromatograph (Agilent Technologies 6890N) for quantitative analyses through a pre evacuated gas transfer line. The transfer lines were purged with the post shocked mixture for sufficient time to flush out any gases that were present. Neither the reactant (MB) nor any of the products (methane, ethane, ethylene, propylene, acetylene, 1,3-butadiene and methyl acrylate) were condensed on the walls as their vapour pressures are very high at room temperature. In addition, the partial pressures of all these compounds in the reaction mixture were much less when compared with their vapour pressures. Therefore, the transfer lines were not heated to avoid any condensation. Lighter compounds (C_1-C_4) were more efficiently separated in a 2 m long packed alumina column.

Heavier gas components were separated in 2 m long Porapak-Q column. The oven temperature was programmed from 35^0C to 150^0C in both the cases. Nitrogen was used as a carrier gas in the analyses. The sensitivity of the flame ionization detector (FID) towards all the reactants and products were calibrated over a known range of concentrations. The concentration/mole fraction of left-out reactant and other products were calculated using the known sensitivity factors obtained in the calibration and the areas under each peak. Parallelly, the samples were analyzed qualitatively in FTIR spectrometer (Bruker's VERTEX 70).

3. Materials and chemicals

MB (99%), methyl acrylate (99%) purchased from Sigma Aldrich and CH_3CF_3 (99% purity) were from SynQuest Laboratories were used in these experiments. MB was further purified by several cycles of freeze-pump-thaw method. Chromatograms of procured samples did not show any products that appeared in the post shock mixtures. Methane (99.5%), ethylene (99.5%), ethane (99.5%), propylene (99.5%), 1, 3-butadiene (99.5%) and high purity helium gas (99.995%) were purchased from Praxair and were used as such in our experiments without further purification.

4. Computational

4.1. Quantum chemical calculations

All electronic structure calculations were carried out using the Gaussian 09 program suite.[25] The geometries of all stationary points on potential energy surface of MB decomposition pathways were optimized with M06-2X level of theory with recommended 6-31+G(d,p) basis set.[26,27] The geometries of the reactant, transition states and products at M06-2X/6-31+G(d,p) level of theory are presented in Figure 2. This functional was verified to be performed well in predicting geometries and vibrational frequencies.[28-30] This functional is also reported to produce

excellent results for reaction kinetics of gas phase reactions and was reported that the calculated rate coefficients in general are very good in agreement with the experimentally measured rate coefficients.[28-30] The normal modes of reactants, transition states and products were viewed in Gauss View.[31] All the reactants and products were confirmed with zero imaginary frequencies (NImag=0), and transition states were confirmed with one imaginary frequency (NImag=1). The minimum energy path (MEP) was obtained by intrinsic reaction coordinate[32] (IRC) calculations using M06-2X/6-31+G(d,p) to verify that the transition states connect the designated reactants and products. By employing the POLYRATE2008[33] GAUSSRATE2009A[34] programs, the theoretical rate coefficients were calculated over the wide temperature range of 500-2500 K using the canonical variational transition state theory[35-37] (CVT) with small-curvature tunneling[38,39] (SCT) method.

$$k^{GT}(T,s) = \sigma \frac{k_B T}{h}\left(\frac{Q^{GT}(T,s)}{Q^{R}(T)}\right) exp\left(\frac{-V_{MEP}(S)}{k_B T}\right)$$

$$k^{CVT}(T) = min_s k^{GT}(T,s) = k^{GT}[T, S^{CVT}(T)]$$

In these equations, k^{GT} and k^{CVT} are the rate coefficients of generalized and canonical variational transition state theories respectively, 's' is reaction path degeneracy, k_B is Boltzmann's constant, h is Planck's constant, T is temperature in Kelvin, S^{CVT} is the reaction coordinate (s) at which canonical variational transition state dividing surface was found. Q^{GT} and Q^{R} are the partition functions of a generalized TS at 's' and reactants respectively. $V_{MEP}(s)$ is the potential energy of generalized TS at 's'. The canonical variational transition state is located by maximizing the free energy of activation with respect to 's'.

4.2 Electronic structures and energetics

A total of six transition states were identified and optimized. These transition states correspond to six different reactions where intramolecular hydrogen transfer happen, *vide infra*. The relative energies ($\Delta E^{\ddagger}_0$ in kcal mol^{-1}) obtained for all TSs using different level of theories are summarized in Table 1. The vibrational frequencies and structural parameters of various species involved in the six reaction pathways obtained at the M06-2X/6-31+G(d,p) level of theory are given in the Supporting Information, SI (Tables S-I to S-II). The potential energy surface is shown in Figure 3 in which all the possible transition states and products are labeled. All the six proposed reactions are pictorially represented along with the corresponding structures in Figure 4. This Figure illustrates the intramolecular hydrogen transfer reactions in thermal decomposition of MB, and the corresponding six reaction channels.

The reaction R1 proceeds through a hydrogen transfer from C1 to O12 through a six-membered transition state TS1, leading to the formation of products P1 (methyl 1-hydroxy vinyl ether) and P2 (Ethylene) through a keto-enol isomerization process. In TS1, the breaking C-H, C-C bond lengths and forming O-H bond lengths are increased by about 38%, 45% and 17% when compared to the C-H, C-C bond in MB and O-H bond in product P1 respectively. This pathway is the low barrier pathway with a barrier height of 67.4 kcal mol^{-1}, which is in very good agreement with the values reported earlier in the literature.[19,40] The relative energy of the products P1 and P2 is 53.4 kcal mol^{-1}.

In reaction R2, a hydrogen transfer occurs from C1 to C6 via four membered transition state TS2, followed by the breaking of C2-C6 bond leading to the formation of products P3 (Ethylene) and P4 (methyl acetate). In transition state TS2, the breaking C-H, C-C bond lengths

and forming C-H bond lengths are increased by about 27%, 51% and 63% when compared to the regular C-H, C-C bond lengths in MB and forming C-H bond length in product P4 respectively. The barrier height (104.8 kcal mol^{-1}) for this reaction is significantly higher compared to those of other reaction pathways (except reaction R6). The reported barrier heights for this channel are in good in agreement with the present study. The relative energy of the products P3 and P4 is 25 kcal mol^{-1}.

The hydrogen transfer in reaction R3 take place from C6 to O12 via transition state TS3. The breaking C-H bond and forming O-H bond lengths are increased by 39% and 29% when compared to the normal C-H bond length in MB and O-H bond length in product P5 (1-hydroxy-1-methoxy-1-butene) respectively. The barrier height for this reaction is 71 kcal mol^{-1}. The barrier height for this reaction is also in good agreement with the one reported by Ali and Violi.[19] The reaction energy for the formation of product P5 is 28 kcal mol^{-1}. In reaction R4, The hydrogen transfer occurs from C6 to O13 through transition state TS4 leading to the formation of products P6 (ethyl ketene) and P7 (methanol), whose relative energy is 28 kcal mol^{-1}, and the barrier energy for the reaction is 73 kcal mol^{-1}. The hydrogen transfer from carbon atom to oxygen atom is less favorable than in the reaction R3. In TS4, the breaking C-H bond length and forming O-H bond length are increased by 37% and 24% when compared to C-H normal bond length in MB and O-H bond length in product P6.

In reaction R5, due to intramolecular hydrogen transfer from C14 to C11 via four centered transition state TS5 followed by breaking of C11-O13 bond in MB. The barrier height for this pathway is 81 kcal mol^{-1}. The primary products formed in the reaction are P8 (butyraldehyde) and P9 (formaldehyde) with relative energy 36 kcal mol^{-1}. In TS5, breaking C-H and C-O bond lengths are increased by 29% and 21% when compared to C-H and C-O bond

lengths in MB. The formed C-H bond is increased by 28% when compared with the C-H bond length in product P8. Similarly in the case of reaction R6, the transfer of hydrogen from C14 to O12 through a five membered transition state TS6 leading to the formation of products P10 (1-butanol radical) and P11 (formaldehyde) with relative energy of 86 kcal mol^{-1}. The barrier energy for this reaction pathway is 105 kcal mol^{-1}, which is significantly higher barrier and less possible reaction compared to all other reaction pathways in current study. The breaking C-H, C-O bond lengths are increased by 42% and 58% when compared to C-H, C-O bond lengths in MB. The forming O-H bond length is increase by 16% when compared to O-H bond length in product P10. The relative energy of the products P10 and P11 is 86 kcal mol^{-1}.

The reaction enthalpies and Gibbs's free energies for thermal decomposition of MB were calculated at M06-2X/6-31+G(d,p) to predict the spontaneity. The values of $\Delta H^0_{298\ K}$ (kcal mol^{-1}) and $\Delta G^0_{298\ K}$ (kcal mol^{-1}) are given in Table 2. All studied reaction pathways (R1-R6) are endothermic and non spontaneous reactions at room temperature. However, these reactions become important with the increase in temperature. Therefore, they are considered in this study, as the working temperatures of this study are in the range of 1229-1427 K.

4.3 Kinetic analysis

Rate coefficients for reactions R1-R6 were computed using canonical variational transition state theory with small curvature tunneling (CVT/SCT) in the temperature range of 500-2500 K. The Arrhenius plot for the computed rate coefficients for reaction pathways R1-R6 at M06-2X/6-31+G(d,p) level of theory in the temperature range of 500-2500 K is shown in Figure 5. The temperature dependent rate coefficients for all the pathways were fit by linear least-squares method and the parameters are tabulated in Table 3. Among all the intramolecular

hydrogen transfer reactions of MB, reactions R1 and R3 showing higher rate coefficients, and reaction R6 is found to have lower rate coefficients. To validate our results, we compared the rate coefficients of reactions R1-R5 with the values reported by Ali and Violi[19] as shown in Figure 5 and the agreement between these two studies seems to be very good.

The overall rate coefficient for the decomposition of MB was obtained by summing the rate coefficients of individual unimolecular reaction channels at the respective temperatures. The overall rate coefficients are plotted along with the experimentally measured rate coefficients for the complete decomposition of MB in Figure 10. The data reported by Ali and Violi[19] was appended to this plot. To our surprise, the agreement between all these rate coefficients is excellent. Therefore, it can be concluded from our theoretical calculations that, the unimolecular reaction channels (R1-R6) mostly governs the reaction. The theoretically calculated rate coefficients were used to fit the Arrhenius equation in the studied temperature range using linear least square method. The temperature dependent Arrhenius expression for the title reaction was obtained to be k_{total}^{theory}(500-2500 K) = (9.05 ± 1.91) × 10^{13} exp (-(70.7 kcal mol^{-1} ± 2.0)/RT) s^{-1}. Also, the computed rate coefficients are in very good agreement with experimentally measured rate coefficients in the temperature range of 1229-1427 K. The rate coefficients computed using the theoretical methods in the present study are for the intramolecular hydrogen transfer reactions, via which the MB decomposes to form majority of the products. However, the rest of the products, methane in particular can be explained only via C-C, C-O and C-H bond scission channels. These channels were not explored theoretically in the present study. The rate coefficients for the rest of all the possible reaction pathways such as C-C, C-O and C-H bond scissions were taken from the literature for the purpose of kinetic simulations, *vide infra*. Therefore, the theoretically calculated temperature dependent rate coefficient is because of the

intramolecular hydrogen transfer reactions alone. However, the temperature dependent rate coefficient deduced using the experimental data is due to all the possible channels. Therefore, the activation energy obtained using theoretical methods is higher when compared with that of the experimentally obtained one. The activation energy can be lowered, if all the possible channels can be optimized using theoretical methods, which is a very difficult task. This may be the main reason for large difference in activation energy for the overall decomposition rate between experiments and theory.

5. Results and discussion

To understand the decomposition mechanism and distribution of reaction products, 35 experiments were carried out with gas mixtures containing 2% of MB and 0.2% of diluted CH_3CF_3 in argon, covering the temperature range of 1229-1427 K. Detailed conditions of each experiment and the normalized yields of products are given in Table 4. The detectable products that were observed in the decomposition of MB and CH_3CF_3 are methane (CH_4), ethane (C_2H_6), ethylene (C_2H_4), acetylene (C_2H_2), 1,1-difluoroethylene (CH_2CF_2), propylene (C_3H_6), 1,3-butadiene (C_4H_6) and methyl acrylate ($C_4H_6O_2$). The product CH_2CF_2 originates from the decomposition of CH_3CF_3 which was used as an internal standard. The other products CH_4, C_2H_6, C_2H_4, C_2H_2, C_3H_6, C_4H_6, and $C_4H_6O_2$ are formed from the decomposition of MB. To confirm this, MB alone was decomposed behind the reflected shock waves in the studied temperature range and confirmed the formation of all these products in the GC analyses of the post shock mixture. Typical chromatograms of the post shocked mixture of an experiment carried out at 1378 K are shown in Figures 6 and 7. The concentration ratios of CH_2CF_2 and CH_3CF_3 were used to determine the temperatures behind the reflected shock waves.

FT-IR analyses were carried out to find out the products formed in the post shock mixture, qualitatively. A representative FT-IR spectrum of the post shock mixture of MB in argon, decomposed at 1378 K is shown in Figure 8. The spectrum shows the presence of MB with a band at 1825 cm^{-1}, and bands in the region 2900-3050 cm^{-1}. The bands in the region 2050-2220 cm^{-1} show the presence of CO, The bands assigned at 3250-3300 cm^{-1} and band with high intensity at 750 cm^{-1} shows the presence of acetylene.

The decay of the reactant and formation of all the products are shown as a function of temperature in Figure 9 with filled circles. The concentrations of the products except methyl acrylate were observed to be increasing with the temperature. However, the concentration of methyl acrylate was observed to be increasing upto 1400 K and then started decreasing with the temperature. The maximum yields for the products methane, ethane, ethylene, acetylene, propylene, 1, 3-butadiene and methyl acrylate were 33%, ~3%, 21%, 36%, ~3%, ~1% and 3% respectively. The product distribution profiles were later compared with the concentration profiles obtained using kinetic simulations, *vide infra*. Figure 9a-h shows the comparisons between the concentrations of products based on analyses of post shock mixtures and those from kinetic simulation with the reaction scheme given in Table 5, *vide infra*. The solid symbols in the Figure are experimental points, and the open symbols represent the simulated ones. The agreement between the experimental concentrations and the simulated values are observed to be good.

The rate coefficients for the overall decomposition of MB were calculated as a first-order rate constant from the relation.

$$k_{total} = -ln\{[MB]_t/[MB]_0\}/t$$

Where $[MB]_t$ and $[MB]_0$ are the experimentally quantified concentrations of MB at the end of the reaction time 't' and 't=0' (initial concentration) respectively. The obtained rate coefficients were used to plot the Arrhenius equation and it is shown in Figure 10. The data were fit using linear least square method and the obtained rate coefficient for overall decomposition of MB in the entire temperature range is k_{total} (1229-1427 K) = (3.08 ± 1.11) × 10^{12} exp (-(53.6 kcal mol^{-1} ± 4.7)/RT) s^{-1}, where R is expressed in the units of kcal $K^{-1}mol^{-1}$. The obtained Arrhenius parameters for the overall decomposition of MB in present experimental and the theoretical study are given in Table 6.

The rate coefficients for the formation of ethylene were computed by using the following relation.[41]

$$k_{ethylene} = \frac{[ethylene]_t}{[MB]_0 - [MB]_t} \times k_{total}$$

where $[ethylene]_t$ is the concentration of ethylene at the end of reaction time 't'. The experimentally obtained rate coefficients were used to plot the Arrhenius equation and are given in Figure 11. The data were fit using linear least squares method and the temperature dependent rate coefficient for the formation of ethylene was obtained to be $k_{ethylene}$ (1229-1427 K) = (7.92 ± 2.72) × 10^{9} exp (-(47.6 kcal mol^{-1} ± 4.5)/RT) s^{-1}. Figure 11 shows the measured rate coefficients for the formation of ethylene from the decomposition of MB in the present experimental and theoretical study along with the RRKM/ME study of Ali and Violi.[19] The present experimental and theoretical rate parameters for the formation of ethylene in the studied temperature range are given in Table 6. The experimentally measured rate coefficients are very good in agreement with available literature rate coefficients and computed rate coefficients of present study in the experimental temperature range of 1229-1427 K.

The error analysis was carried out to estimate the overall uncertainty of the experimentally measured rate coefficients in the studied temperature range. The main contributions to the overall uncertainty in the measured rate coefficients considered in the error analyses are (a) initial temperature T_1 (±1%) (b) The uncertainty reported in the internal standard reaction rate coefficient (±23%), (c) concentration measurements (±1%) and (d) The fitting error in Arrhenius plot (±2%). The uncertainties were combined in a root-sum-squared method to give an overall (σ) uncertainty of ± 23% in the present experiments.

5.1. Kinetic simulations

To understand the reaction mechanism and also to model the observed distribution of reactant and products, a kinetic scheme was proposed and it is given in Table 5. The reaction scheme contains 39 species including 66 elementary reactions was proposed in the present study. The reaction mechanism proposed earlier by Huynh *et al.*[42] was also included in the present kinetic scheme. The rate coefficients for reactions R1-R6 are taken from the present theoretical study and rate coefficients for all other reactions are taken from literature.[42-50] The rate coefficients listed in the Table 5 are given in $k = A\exp(-E_a/RT)$ or $k = AT^n\exp(-E_a/RT)$ formats, where A factors are given in s^{-1} and $cm^3\ mol^{-1}\ s^{-1}$ for first and second order reactions respectively, and activation energies are given in kcal mol^{-1}. Kinetic simulations are carried out at experimentally determined temperatures and reaction times. The concentrations obtained in the simulations using the proposed reaction mechanism are plotted along with the experimentally measured concentrations in Figure 9a-h. The major products in the decomposition of MB are methane (33%), ethylene (21%) and acetylene (36%). In case of these major products, the agreement between the experimental and simulated concentrations was found to be very good. The minor products are ethane (3%), propylene (3%), 1,3-butadiene (1%) and methyl acrylate

(3%). The agreement between the experimentally measured and simulated concentrations was found to be good in case of ethane and propylene. However, the agreement is not good only in case of 1,3-butadiene and methyl acrylate. As the concentrations of these two compounds are very low, the agreement could not be achieved with the proposed mechanism.

In high temperature conditions, the initiation step for the decomposition of MB is expected via unimolecular reactions and bimolecular hydrogen abstraction reactions. The unimolecular reactions proceed through two types of reactions. First type of reactions are bond fission reactions (R7, R8, R9, R10, and R11) and second type of reactions are multiple bond fission reactions (R1, R2, R3, R4, R5, and R6). The bimolecular hydrogen abstraction reactions by reactive radicals such as H atoms and $CH_3^{\bullet}$ radicals are the other channels via which the decomposition happen.

Initially, four methyl butanoate radicals are formed via hydrogen abstraction reactions R12, R13, R14 and R15 (cf the reaction scheme). These radicals can isomerizes through hydrogen migration reactions. For example, $CH_2^{\bullet}$-CH_2-CH_2-C(O)-O-CH_3 radical can be isomerized to CH_3-$CH^{\bullet}$-CH_2-C(O)-O-CH_3, CH_3-CH_2-$CH^{\bullet}$-C(O)-O-CH_3, CH_3-CH_2-CH_2-C(O)-O-$CH_2^{\bullet}$ through 1-2, 1-3, and 1-6 hydrogen migration reactions. Similarly, CH_3-$CH^{\bullet}$-CH_2-C(O)-O-CH_3 radical can be isomerized to CH_3-CH_2-$CH^{\bullet}$-C(O)-O-CH_3 and CH_3-CH_2-CH_2-C(O)-O-$CH_2^{\bullet}$ through 1-2 and 1-5 hydrogen migration reactions, respectively. The 1-4 hydrogen migration is responsible for the transformation between radicals CH_3-CH_2-$CH^{\bullet}$-C(O)-O-CH_3 and CH_3-CH_2-CH_2-C(O)-O-$CH_2^{\bullet}$. The radical isomerization reactions through hydrogen migration in the reaction scheme are not sensitive reactions. These reactions are included in the reaction scheme for completeness of mechanism.

5.1.1. Methane

The maximum concentration of methane was found to be 33% in the studied temperature range. The formation of methane can be explained by the formation of methyl radicals in the decomposition of MB. The formed methyl radicals abstract hydrogen atom from four different sites of MB by forming methyl butanoate radicals and methane through reactions R20, R21, R22, and R23. The barrier height of the hydrogen abstraction reaction at any of these specific sites by the methyl radical is reported[42] to be less than 8 kcal mol^{-1}.

$MB + CH_3^{\bullet} \rightarrow CH_3\text{-}CH_2\text{-}CH_2\text{-}C(O)\text{-}O\text{-}CH_2^{\bullet} + CH_4$

$$k_{20} = 2.28 \times 10^{-8} (T)^{5.88} \exp(-6.79/RT)\ cm^3mol^{-1}s^{-1} \quad \text{(R20)}$$

$MB + CH_3^{\bullet} \rightarrow CH_2^{\bullet}\text{-}CH_2\text{-}CH_2\text{-}C(O)\text{-}O\text{-}CH_3 + CH_4$

$$k_{21} = 1.50 \times 10^{4} (T)^{2.96} \exp(-4.29/RT)\ cm^3mol^{-1}s^{-1} \quad \text{(R21)}$$

$MB + CH_3^{\bullet} \rightarrow CH_3\text{-}CH^{\bullet}\text{-}CH_2\text{-}C(O)\text{-}O\text{-}CH_3 + CH_4$

$$k_{22} = 1.44 \times 10^{-5} (T)^{4.97} \exp(-7.18/RT)\ cm^3mol^{-1}s^{-1} \quad \text{(R22)}$$

$MB + CH_3^{\bullet} \rightarrow CH_3\text{-}CH_2\text{-}CH^{\bullet}\text{-}C(O)\text{-}O\text{-}CH_3 + CH_4$

$$k_{23} = 1.87 \times 10^{-5} (T)^{4.97} \exp(-6.06/RT)\ cm^3mol^{-1}s^{-1} \quad \text{(R23)}$$

The revere reactions generate methyl radicals in the backward reaction. Therefore, reactions R24, R25, R26, and R27 are added in the reaction scheme for completeness.

$CH_3\text{-}CH_2\text{-}CH_2\text{-}C(O)\text{-}O\text{-}CH_2^{\bullet} + CH_4 \rightarrow MB + CH_3^{\bullet}$

$$k_{27} = 3.02 \times 10^{-7} (T)^{5.48} \exp(-12.39/RT)\ cm^3mol^{-1}s^{-1} \quad \text{(R27)}$$

$CH_2^{\bullet}$-CH_2-CH_2-C(O)-O-CH_3 + CH_4 → MB + $CH_3^{\bullet}$

$$k_{24} = 2.22 \times 10^{1} (T)^{3.26} \exp(-9.06/RT)\ cm^3mol^{-1}s^{-1} \quad (R24)$$

CH_3-$CH^{\bullet}$-CH_2-C(O)-O-CH_3 + CH_4 → MB + $CH_3^{\bullet}$

$$k_{25} = 4.35 \times 10^{-8} (T)^{5.59} \exp(-13.85/RT)\ cm^3mol^{-1}s^{-1} \quad (R25)$$

CH_3-CH_2-$CH^{\bullet}$-C(O)-O-CH_3 + CH_4 → MB + $CH_3^{\bullet}$

$$k_{26} = 1.24 \times 10^{-7} (T)^{5.71} \exp(-17.24/RT)\ cm^3mol^{-1}s^{-1} \quad (R26)$$

The sensitivity of each reaction towards the formation and decomposition of CH_4 was carried out by varying the rate coefficients of each reaction by a factor of 10. The results are shown in Figure 12 in terms of percentage change in the concentrations with respect to the reaction numbers. The reactions R20 and R21 are observed to be very sensitive in the formation of CH_4. In both these channels CH_3 radical is key species for the decomposition of MB. Reactions R7, R15, R17 and R42 have shown significant influence on the formation of methane.

5.1.2. Ethylene

The other major product is C_2H_4, which is formed mainly via direct decomposition of MB through a 6 membered transition state (TS1 through reaction R1) and a four membered transition state (TS2 through reaction R2) (cf Figure 2). Concentrations of C_2H_4 were found to be lower than the concentrations of CH_4 by 10% in the studied temperature range. Ethylene is formed through reactions R1 and R2 and rate coefficients for these channels are computed theoretically in the present investigation. The activation energies for these two reactions R1 and R2 were calculated to be 68 and 106 kcal mol^{-1} respectively. Therefore, it is obvious that reaction R1 contribute more to the formation of ethylene when compared to that of R2.

$MB \rightarrow C_2H_4 + CH_2{=}C(OH)\text{-}O\text{-}CH_3 \quad k_1 = 1.62 \times 10^{13} \exp(-68.46/RT)\ s^{-1}$ (R1)

$MB \rightarrow CH_3\text{-}C(O)\text{-}O\text{-}CH_3 + C_2H_4 \quad k_2 = 2.51 \times 10^{13} \exp(-106.30/RT)\ s^{-1}$ (R2)

The other main contribution for the formation of ethylene is reaction R26. The ethylene is formed via β-C-C bond scission of $CH_2^{\bullet}\text{-}CH_2\text{-}CH_2\text{-}C(O)\text{-}O\text{-}CH_3$ radical.

$CH_2^{\bullet}\text{-}CH_2\text{-}CH_2\text{-}C(O)\text{-}O\text{-}CH_3 \rightarrow C_2H_4 + CH_2^{\bullet}\text{-}C(O)\text{-}O\text{-}CH_3$

$k_{26} = 5.25 \times 10^{11} (T)^{0.50} \exp(-26.59/RT)\ s^{-1}$ (R26)

The reaction between two methyl radicals to form ethylene (R55) is added to the reaction scheme for completeness.

$2\ CH_3^{\bullet} \rightarrow C_2H_4 + H_2 \quad k_{55} = 9.90 \times 10^{15} \exp(-32.98/RT)\ cm^3mol^{-1}s^{-1}$ (R55)

Ethylene reacts with hydrogen atoms and form $C_2H_3^{\bullet}$ radical and H_2 through reaction R65, which is main source for the formation acetylene.

$C_2H_4 + H \rightarrow C_2H_3^{\bullet} + H_2 \quad k_{65} = 5.24 \times 10^{14} \exp(-14.90/RT)\ cm^3mol^{-1}s^{-1}$ (R65)

The sensitivity analysis of the proposed reaction scheme is carried out for the formation of C_2H_4 and the results are shown in Figure 12. Reactions R1, R13, and R50 are very sensitive to the formation of C_2H_4.

5.1.3. Acetylene

Acetylene is one of the major products obtained in the thermal decomposition of MB. The measured concentration of acetylene is 36% in the present experimental study. The radical $CH^{\bullet}{=}CHC(O)OCH_3$ can produce C_2H_2 by C-C(O) bond cleavage. The radical $CH^{\bullet}{=}CH\text{-}C(O)\text{-}O\text{-}$

CH_3 is formed by hydrogen abstraction from $=CH_2$ group of CH_2=CH-C(O)-O-$CH_2^{\bullet}$ (This radical in turn is formed via γ-C-C bond scission of methyl butanoate radical through reaction R43) through reaction R46. The other possibility for the formation of acetylene and hydrogen atom is via decomposition of $C_2H_3^{\bullet}$ radicals (R63).

$CH^{\bullet}$=CH-C(O)-O-$CH_3 \rightarrow C_2H_2 + CH_3$-O-$C(O)^{\bullet}$

$$k_{24} = 5.76 \times 10^{12} (T)^{0.82} \exp(-38.50/RT)\ cm^3mol^{-1}s^{-1} \quad (R48)$$

$C_2H_3^{\bullet} \rightarrow C_2H_2 + H$ $\quad k_{63} = 2.00 \times 10^{14} \exp(-39.74/RT)\ s^{-1}$ (R63)

The sensitivity analysis is carried out for the formation of C_2H_2 and the results are shown in Figure 13. Reactions R7, R17 and R65 are found to be sensitive for the formation of C_2H_2.

5.1.4. Minor products

The minor reaction products observed in the experiments are ethane (C_2H_6), propylene (C_3H_6), 1,3-butadiene(C_4H_6) and methyl acrylate. The concentrations of these four products are less than 4%, when compared with the main products. The concentrations of ethane, propylene, 1,3-butadiene seems to be increasing with the temperature in the studied temperature range. The concentration of the other minor product methyl acrylate was observed to be increasing upto 1400 K and beyond this temperature it was found to be decreasing. The most possible channels for the formation of C_2H_6 is the recombination of two $CH_3^{\bullet}$ radicals (R54) and reaction between propylene with $C_2H_5^{\bullet}$ radical (R66).

$2\ CH_3^{\bullet} \rightarrow C_2H_6$ $\quad k_{54} = 6.80 \times 10^{14} (T)^{-0.60}\ cm^3mol^{-1}s^{-1}$ (R54)

$C_3H_6 + C_2H_5^{\bullet} \rightarrow C_2H_6 + C_3H_5^{\bullet}$ $\quad k_{66} = 2.23 (T)^{3.50} \exp(-6.64/RT)\ cm^3mol^{-1}s^{-1}$ (R66)

Propylene is formed directly from C-C(O) bond dissociation of CH_3-$CH^{\bullet}$-CH_2-C(O)-O-CH_3 radical (R40). The other channel via which propylene formed is C-H bond scission in n-$C_3H_7^{\bullet}$ radical (R53).

CH_3-$CH^{\bullet}$-CH_2-C(O)-O-CH_3 → C_3H_6 + CH_3-O-$C(O)^{\bullet}$

$$k_{40} = 4.53 \times 10^{12} (T)^{0.33} \exp(-34.27/RT)\ cm^3mol^{-1}s^{-1} \qquad (R40)$$

CH_3-CH_2-$CH_2^{\bullet}$ → C_3H_6 + H $\qquad k_{53} = 4.14 \times 10^{12} (T)^{0.17} \exp(-35.62/RT)\ s^{-1}$ (R53)

On the other hand, propylene reacts with $C_2H_3^{\bullet}$ and $C_2H_5^{\bullet}$ radicals and form 1,3-butadiene and ethane through reactions R62 and R66. The only channel through which 1,3-butadiene can be formed using the present scheme is reaction R62.

C_3H_6 + $C_2H_3^{\bullet}$ → C_4H_6 + $CH_3^{\bullet}$ $\qquad k_{62} = 7.23 \times 10^{11} \exp(-5.01/RT)\ cm^3mol^{-1}s^{-1}$ (R62)

Methyl acrylate is formed by breaking C-C bond of CH_3-CH_2-$CH^{\bullet}$-C(O)-O-CH_3 through a β-scission (R42). It is also formed by C-H bond scission at α-position of $CH_2^{\bullet}$-CH_2-C(O)-O-CH_3 through reaction R43. These two reactions are responsible for the formation of methyl acrylate in these experimental conditions.

CH_3-CH_2-$CH^{\bullet}$-C(O)-O-CH_3 → CH_2=CH-C(O)-O-CH_3 + $CH_3^{\bullet}$

$$k_{42} = 1.33 \times 10^{11} (T)^{0.97} \exp(-34.88/RT)\ s^{-1} \qquad (R42)$$

$CH_2^{\bullet}$-CH_2-C(O)-O-CH_3 → CH_2=CH-C(O)-O-CH_3 + H

$$k_{43} = 1.53 \times 10^{8} (T)^{1.57} \exp(-38.38/RT)\ s^{-1} \qquad (R43)$$

Sensitivity analysis is carried out to check the sensitivity of each reaction towards the formation and decomposition of minor products by varying the rate coefficients of each proposed reaction by a factor of 10. The results are shown in Figure 14 and Figure 15 in terms of percentage changes in the concentrations with respect to the reaction numbers. The reactions R7, R8 and R24 are sensitive for the formation of C_2H_6. It shows methyl radicals are key species for the formation of C_2H_6. Reactions R14 and R40 have shown more sensitivity towards the formation of C_3H_6. The reactions R7, R8, R21, R44 and R65 have shown more sensitivity towards the formation of 1,3-butadiene. In the case of methyl acrylate formation, the reactions R12, R15, R42 and R58 are observed to be more sensitive.

It should be noted here that, the agreement between the experimentally measured concentrations and simulated ones was found to be not that satisfactory in case of 1,3-butadiene and methyl acrylate. As the concentrations of these two compounds are very low (1% and 3% respectively), the agreement could not be achieved with the proposed mechanism. As mentioned before, the only channel through which 1,3-butadiene can be formed using the present scheme is reaction R62.

$C_3H_6 + C_2H_3^{\bullet} \rightarrow C_4H_6 + CH_3^{\bullet}$ $\quad k_{62} = 7.23 \times 10^{11} \exp(-5.01/RT)\ cm^3mol^{-1}s^{-1}$ (R62)

Although the amount of propylene available for this reaction is plenty, the formation of 1,3-butadiene is subject to the availability of C_2H_3 radical, whose formation is very minimal. Therefore, the agreement between experiment and simulations is not good, in case of 1,3-butadiene.

Another very important product that we observed in FTIR analysis in the experiments is CO. The contribution for the formation of CO is significant via the reactions R52, R58 and R59.

$CH_2^{\bullet}\text{-}CH{=}CO \rightarrow C_2H_3^{\bullet} + CO$ $\quad k_{52} = 3.47 \times 10^{12}(T)^{0.63} \exp(-27.21/RT)\ s^{-1}$ (R52)

CH_2=C(O) + H → CO + $CH_3^{\bullet}$ k_{58}= 7.77 × 10^8(T)$^{1.45}$exp (-2.78/RT) $cm^3mol^{-1}s^{-1}$ (R58)

CH_3-O-C(O)$^{\bullet}$ → CO + CH_3-O$^{\bullet}$ k_{59}= 8.02 × 10^{11}(T)$^{0.65}$exp (-21.12/RT) s^{-1} (R59)

Sensitivity analysis has show reaction R58 to be more sensitive to the formation of CO.

6. Conclusions

In the present investigation, we have reported the rate coefficients for total decomposition of MB in the temperature range of 1229 – 1427 K, for the first time. The obtained rate coefficient for the total decomposition of MB in the studied temperature range is k_{total} (1229-1427 K) = (3.08 ± 1.11) × 10^{12} exp (-(53.6 kcal mol^{-1} ± 4.7)/RT) s^{-1}. In addition to this we have reported rate coefficients for intramolecular hydrogen transfer reactions (R1-R6) in thermal decomposition of MB using computational methods. The kinetic data calculated for the unimolecular elimination reactions over the temperature range of 500-2500 K were used to derive the Arrhenius expression: k_{total}^{theory}(500-2500 K) = (9.05 ± 1.91) × 10^{13} exp (-(70.7 kcal mol^{-1} ± 2.0)/RT) s^{-1}. The computed rate coefficients for the reactions (R1-R6) were used in kinetic modelling to understand the complete decomposition reaction mechanism. Here, well established theoretical methods are helpful to extrapolate rate coefficients to higher temperatures. The basis of every detailed reaction mechanism in combustion is formed by a set of elementary reactions and its kinetic parameters. The comprehensive modeling of biodiesel combustion requires large amounts of experimental data and extensive investigation on the detailed combustion mechanisms. These rate coefficients obtained in the present study are useful to understand the combustion of large size complex biodiesel molecules by including these elementary reactions in their modelling.

Acknowledgment

B.R. thanks Council of Scientific and Industrial Research (CSIR), Government of India for funding. A.P. is very grateful to CSIR for providing a research fellowship. A.P. also thank Mr. G. Sudhakar and Mr. G. Srinivasulu for their help in doing the experiments.

References

(1) M. Besson, P. Gallezot, and C. Pinel, *Chem. Rev.* 2014, **114,** 1827-1870.

(2) W. K. Metcalfe, S. Dooley, H. J. Curran, J. M. Simmie, A. M. Al-Nahas, and M. V. Navarro, *J. Phys. Chem. A* 2007, **111**, 4001-4014.

(3) R. Behcet, H. Oktay, A. Cakmak, and H. Aydin, *Renewable Sustainable Energy Rev*. 2015, **46,** 157-165.

(4) G. Knothe, C. A. Sharpe, and T. W. Ryan, *Energy Fuels*. 2006, **20**, 403-408.

(5) M. S. Graboski, and R. L. McCormick, *Prog. Energy Combust. Sci*. 1998, **24**, 125-164.

(6) K. Bozbas, *Renewable Sustainable Energy Rev*. 2008, **12,** 542-552.

(7) J. M. Simmie, *Prog. Energy Combust. Sci.* 2003, ***29*,** 599-634.

(8) O. Herbinet, W. J. Pitz, and C. K. Westbrook, *Combust. Flame* 2008, **154,** 507-528.

(9) P. Dievart, S. H. Won, S. Dooley, F. L. Dryer, Y. Ju, *Combust. Flame* 2012, **159,** 1793-1805.

(10) K. Kohse-Hoinghaus, P. Osswald, T. A. Cool, T. Kasper, N. Hansen, F. Qi, C. K. Westbrook, and P. R. Westmoreland, *Angew. Chem.* 2010, **49,** 3572-3597.

(11) S. Gail, M. J. Thomson, S. M. Sarathy, S. A. Syed, P. Dagaut, P. Dievart, A. J. Marchese, and F. L. Dryer, *Proc. Combust. Inst.* 2007, ***31*,** 305-311.

(12) A. Farooq, D. F. Davidson, R. K. Hanson, L. K. Huynh, and A. Violi, *Proc. Combust. Inst.* 2009, **32,** 247-253.

(13) A. Farooq, W. Ren, K.-Y. Lam, D. F. Davidson, R. K. Hanson, and C. K. Westbrook, *Combust. Flame* 2012, **159,** 3235-3241.

(14) K. C. Lin, J. Y. W. Lai, and A. Violi, *Fuel* 2012, **92,** 16-26.

(15) E. M. Fisher, W. J. Pitz, H. J. Curran, and C. K. Westbrook, *Proc. Combust. Inst*. 2000, **28,** 1579-1586.

(16) M. H. Hakka, H. Bennadji, J. Biet, M. Yahyaoui, B. Sirjean, V. Warth, L. Coniglio, O. Herbinet, P. A. Glaude, F. Billaud, and F.Battin- Leclerc, *Int. J. Chem. Kinet*. 2010, **42,** 226-252.

(17) S. Dooley, H. J. Curran, and J. M. Simmie, *Combust. Flame* 2008, **153,** 2-32.

(18) J. Y. W. Lai, K. C. Lin, and A. Violi, *Prog. Energy Combust. Sci*. 2011, **37,** 1-14.

(19) M. A. Ali, and A. Violi, *J. Org. Chem.* 2013, **78,** 5898-5908.

(20) G. Sudhakar, and B. Rajakumar, *J. Chem. Sci*. 2014, **126,** 897-909.

(21) A. G. Gaydon, and I.RHurle, I.R. The Shock Tube in High-Temperature Chemical Physics, Reinhold Publishing, New York, **1963**.

(22) A. Lifshitz, C. Tamburu, and A. Suslensky, *J. Phys. Chem. A* 2006, **110,** 11677-11683.

(23) J. A. Manion, and I. A. Awan, *Proc. Combust. Inst* 2013, ***34*,** 537-545.

(24) M. Akira, Y. Kenji, and S. Hiroumi, *J. Phys. Chem. A* 2014, ***118*,** 11688-11695.

(25) M. J. Frisch, G. W. Trucks, H. B. Schlegel, G. E. Scuseria, M. A. Robb, J. R. Cheeseman, G. Scalmani, V. Barone, B. Mennucci, G. A. Petersson, Gaussian 09, Revision B.01, Gaussian, Inc., Wallingford, CT, 2010.

(26) Y. Zhao, D. G. Truhlar, *Acc. Chem. Res.* 2008, **41,** 157-167.

(27) Zhao, Y.; Truhlar, D. G. *Theor. Chem. Acc*. 2008, **120,** 215-241.

(28) G. Srinivasulu, and B. Rajakumar, *J. Phys. Chem. A* 2013, **117,** 4534-4544.

(29) M. Balaganesh, M. R. Dash and B. Rajakumar, *J. Phys. Chem. A* 2014, **118,** 5272-5278.

(30) M. R. Dash, and B. Rajakumar, *Atmospheric Environment*, 2013, **79,** 161-171.

(31) I. I. R. Dennington, T. Keith, J. Millam, K. Eppinnett, W. L. Hovell, and R. Gilliland, GaussView, Version 3.09, Semichem, Inc., Shawnee Mission, KS, 2003.

(32) C. Gonzalez, H.B. Schlegel, *J. Chem. Phys.* 1989, **90,** 2154-2161.

(33) J. Zheng, S. Zhang, B. J. Lynch, J. C. Corchado, Y.-Y. Chuang, P. L. Fast, W.-P. Hu, Y.-P. Liu, G. C. Lynch, and K. A. Nguyen, POLYRATE, version 2008; University of Minnesota: Minneapolis,MN, 2009.

(34) J. Zheng, S. Zhang, J. C. Corchado, Y.-Y. Chuang, E. L. Coitiño, B. A. Ellingson, and D. G. Truhlar, GAUSSRATE, version 2009-A; University of Minnesota: Minneapolis, MN, 2010.

(35) A. Gonzalez-Lafont, T. N. Truong, and D. G. Truhlar, *J. Chem.Phys*. 1991, **95,** 8875−8894.

(36) B. C. Garrett, and D. G. Truhlar, *J. Phys. Chem*. 1979, ***83*,** 1052-1079.

(37) B. C. Garrett, D. G. Truhlar, R. S. Grev, and A. W. Magnuson, *J. Phys. Chem*. 1980, ***84*,** 1730-1748.

(38) D. H. Lu, T. N. Truong, V. S. Melissas, G. C. Lynch, Y. P. Liu, B. C. Garrett, R. Steckler, A. D. Isaacson, S. N. Rai, and G. C. Hancock, *Comput. Phys.Commun*. 1992, **71,** 235-262.

(39) Y. P. Liu, G. C. Lynch, T. N. Truong, D. H. Lu, D. G. Truhlar, and B. C. Garrett, *J. Am. Chem.Soc*. 1993, **115,** 2408-2415.

(40) A.M. El-Nahas, M. V. Navarro, J. M. Simmie, J. W. Bozzelli, H. J. Curran, S. Dooley, and W. Metcalfe. *J. Phys. Chem. A* 2007, **111,** 3727-3739.

(41) A. Lifshitz, C. Tamburu, A. Suslensky, and F. Dubnikova, *J. Phys. Chem. A* 2004, **108,** 3430-3438.

(42) L. K. Huynh, and A. Violi, *J. Org. Chem*. 2008, **73,** 94-101.

(43) H. J. Curran, *Int. J. Chem. Kinet*. 2006, **38,** 250-275.

(44) A. Lifshitz, C. Tamburu, and A. Suslensky, *J. Phys. Chem*. 1990, **94,** 2966-2972.

(45) R. D. Kern, H. J. Singh, and C. H. Wu, *Int. J. Chem. Kinet*. 1988, **20,**731-747.

(46) D. F. Davidson, M. D. DiRosa, E. J. Chang, R. K. Hanson, and C. T. Bowman, *Int. J. Chem. Kinet*. **1995**, *27*, 1179-1196.

(47) J. P. Senosiain, S. J. Klippenstein, and J. A. Miller, *J. Phys. Chem. A* 2006, **110,** 5772-5781.

(48) H. Hippler, F. Striebel, and B. Viskolcz, *Phys. Chem. Chem. Phys*. 2001, **3,** 2450-2458.

(49) W. Tsang, *J. Phys. Chem. Ref. Data* 1991, **20,** 221-273.

(50) D. L. Baulch, C. J. Cobos, R. A. Cox, C. Esser, P. Frank, T. Just, J. A. Kerr, M. J. Pilling, J. Troe, R. W. Walker, and J. Warnatz, *J. Phys. Chem. Ref. Data*, 1992, **21,** 411-429.

Figure Captions

Figure 1. A typical pressure trace recorded by an oscilloscope showing the arrival of primary, reflected shock waves, reaction time and expansion/cooling wave.

Figure 2. Geometries of the reactant, transition states, and products optimized at the M06-2X/6-31+G(d,p) level of theory. Blue color represents hydrogen and gray color represents carbon, red color represents oxygen in the structures. The bond lengths (Å) given on the structures are obtained at M06-2X/6-31+G(d,p) level of theory.

Figure 3. Potential energy surfaces of reaction channels R1-R6 computed using the M06-2X/6-31+G(d,p) level of theory. The energies are given in the units of kcal mol^{-1}.

Figure 4. The reaction pathways (R1-R6) for the unimolecular decomposition of methyl butanoate considered in this study.

Figure 5. Arrhenius plots for the rate coefficient data obtained for the reaction pathways R1-R6 over the temperature range of 500-2500 K.

Figure 6. Gas chromatogram showing the products of the post shock mixture of the experiment carried out at 1378 K. The peaks labeled in the chromatogram are A: methane, B: ethylene, C: ethane, D: propylene, E: acetylene, F: 1,3-butadiene, G: methyl acrylate, and H: methyl butanoate.

Figure 7. Gas chromatogram showing the products of the post shock mixture of the experiment carried out at 1378 K. The peaks labeled in the chromatogram are (a) methane (b) ethane (c) ethylene (d) 11-DFE (e) acetylene (f) 111-TFE (g) propylene.

Figure 8. FTIR spectrum of the post shock mixture of methyl butanoate diluted in argon pyrolyzed at 1378 K. All the peaks are assigned to (A) methyl butanoate, (B) methane, (C) ethylene, (D) ethane., (E) acetylene, (F) propylene (G) methyl acrylate (H) CO

Figure 9. Comparison between the experimentally measured and simulated concentrations of (a) methyl butanoate, (b) methane, (c) ethylene, (d) acetylene, (e) ethane, (f) propylene (g) 1,3-butadiene (h) methyl acrylate. Filled circles on the plot are experimental concentrations and the open circles are simulated concentrations.

Figure 10. Arrhenius plot for the overall decomposition of methyl butanoate in the temperature range of 1229-1427 K. The obtained temperature dependent rate coefficient for the entire experimental temperature range is k_{total} (1229-1427 K) = (3.08 ± 1.11) × 10^{12} exp (-(53.6 kcal mol^{-1} ± 4.7)/RT) s^{-1}. The insert is the zoom of the data obtained in the present experiments.

Figure 11. Arrhenius plot for the formation of ethylene in the decomposition of methyl butanoate. The obtained temperature dependent rate coefficient for the entire experimental temperature range is $k_{ethylene}$ (1229-1427 K) = (7.92 ± 2.72) × 10^{9} exp (-(47.6 kcal mol^{-1} ± 4.5)/RT) s^{-1}. The insert is the zoom of the data obtained in the present experiments.

Figure 12. Sensitivity analysis of the proposed reaction scheme carried out at 1347 K for the formation of methane and ethylene.

Figure 13. Sensitivity analysis of the proposed reaction scheme carried out at 1347 K for the formation of acetylene and CO.

Figure 14. Sensitivity analysis of the proposed reaction scheme carried out at 1347 K for the formation of ethane and propylene.

Figure 15. Sensitivity analysis of the proposed reaction scheme carried out at 1347 K for the formation of 1,3-butadiene and methyl acrylate.

Table Captions

Table 1. Energy barriers (kcal mol^{-1}) for thermal decomposition of methyl butanoate reaction via pathways R1-R6, calculated at M06-2X/6-31+G(d,p).

Table 2. The reaction enthalpies ($\Delta H^0_{298\ K}$, kcal mol^{-1}), free energies ($\Delta G^0_{298\ K}$, kcal mol^{-1}) are calculated at M06-2X/6-31+G(d,p) level of theory.

Table 3. Arrhenius parameters for thermal decomposition of methyl butanoate via reaction pathways (R1-R6) in the temperature range of 500-2500 K.

Table 4. Experimental conditions and distribution of normalized concentrations of reactant and reaction products in the decomposition of methyl butanoate.

Table 5. Proposed reaction scheme for the decomposition of methyl butanoate with 39 reaction species and 66 elementary reactions.

Table 6. The present experimental and theoretical rate parameters for total decomposition of methyl butanoate and formation of ethylene in the studied temperature range.

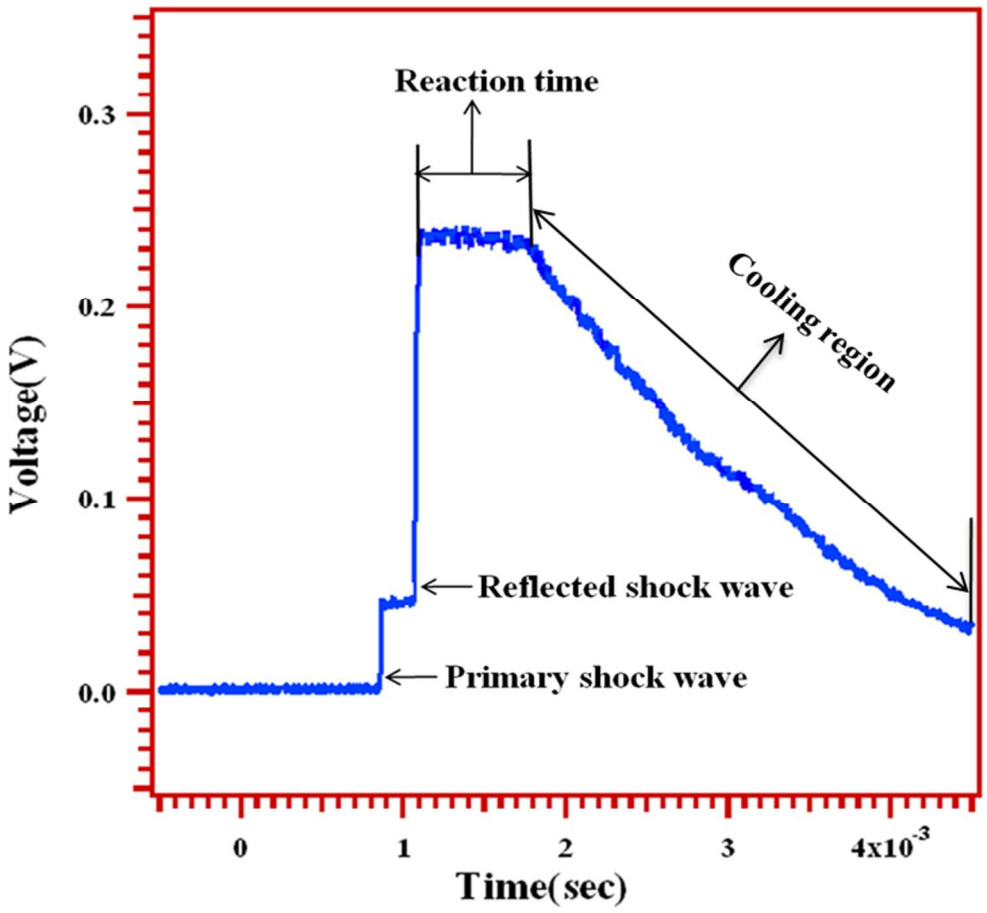

Figure 1. A typical pressure trace recorded by an oscilloscope showing the arrival of primary, reflected shock waves, reaction time and expansion/cooling wave.

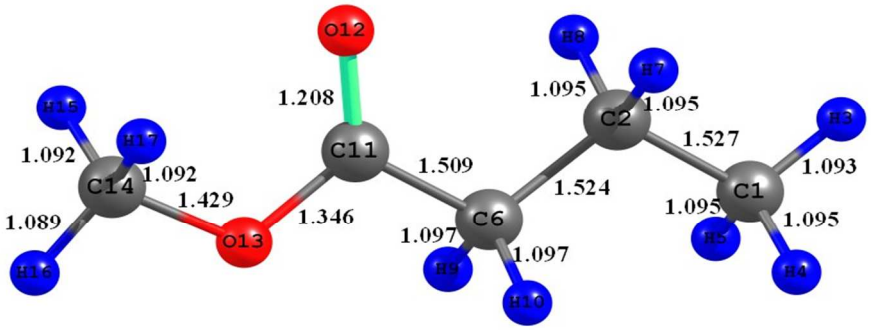

Methyl butanoate (MB)

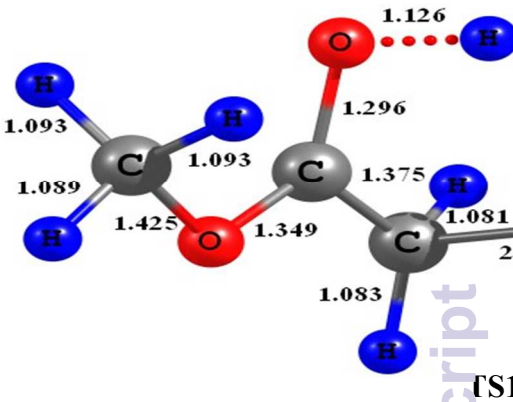

TS1

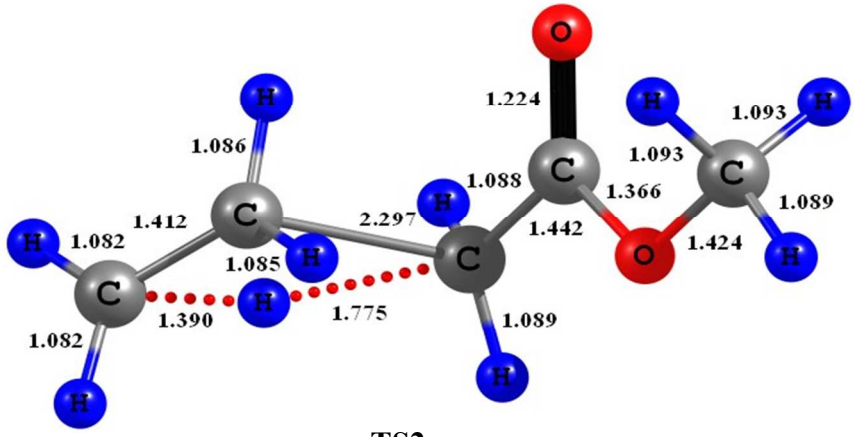

TS2

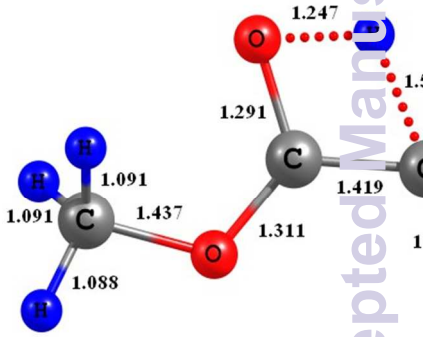

TS3

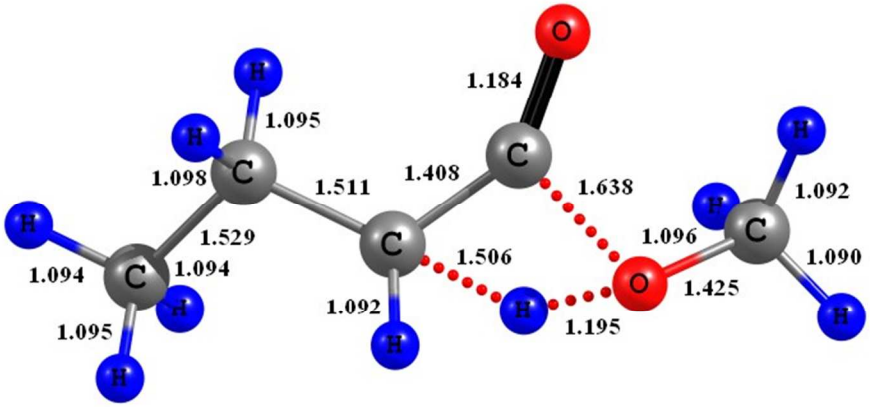

TS4

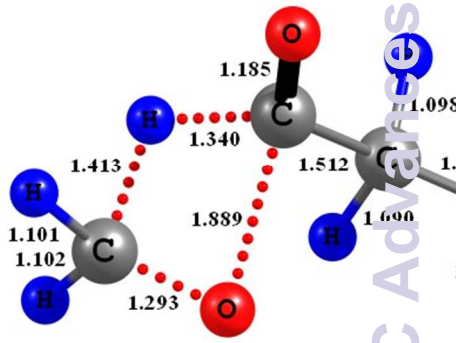

TS5

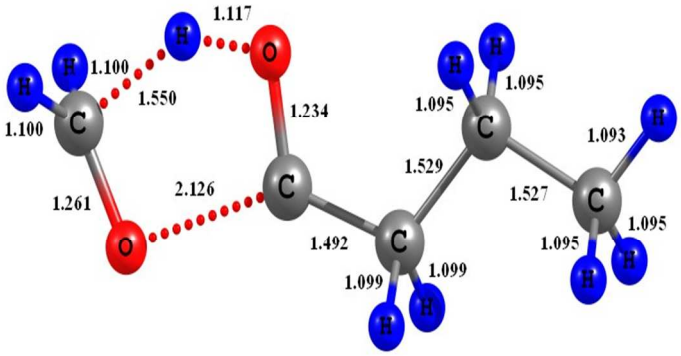

TS6

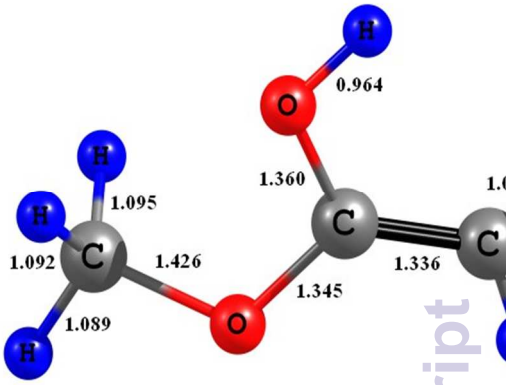

P1

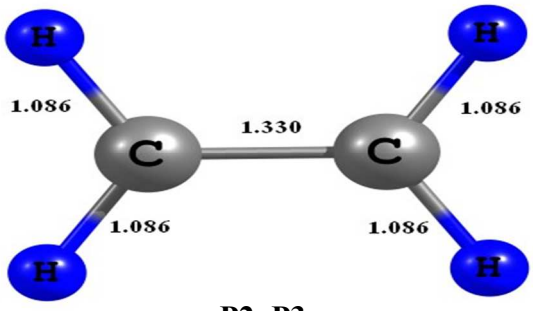

P2, P3

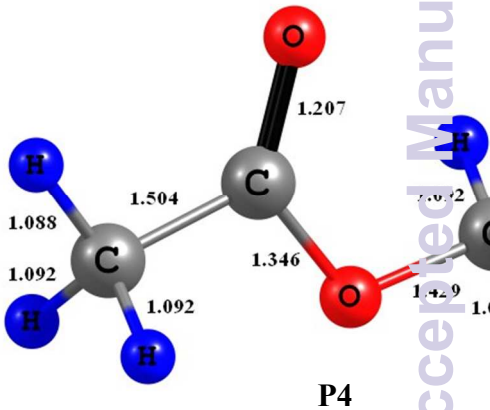

P4

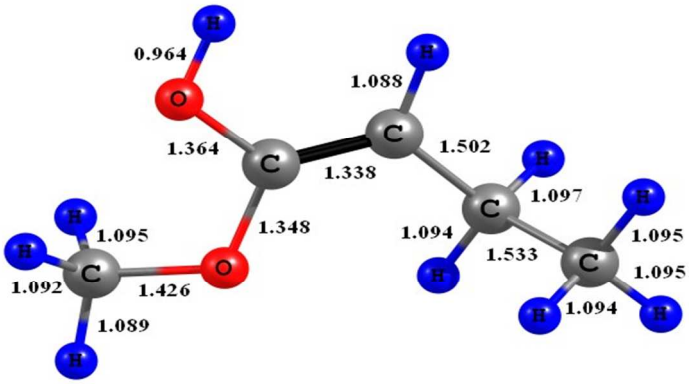

P5

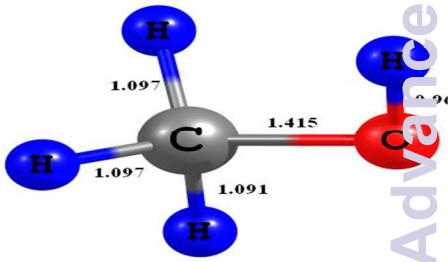

P7

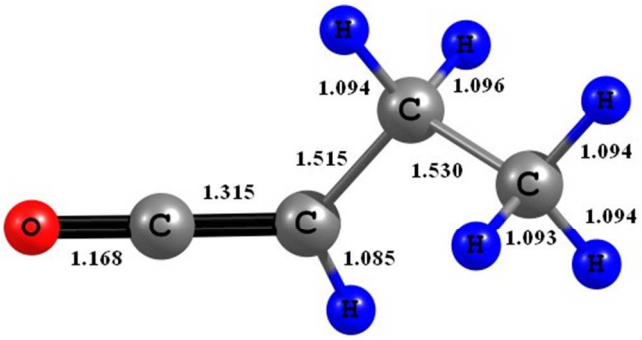

P6

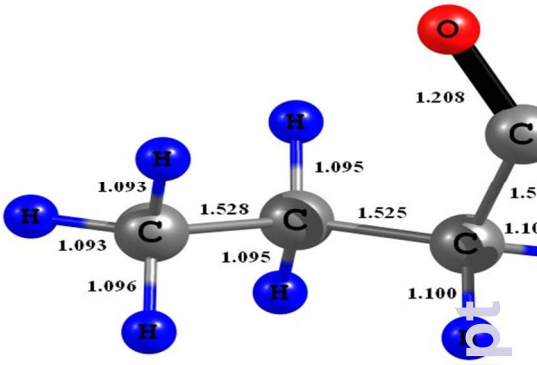

P8

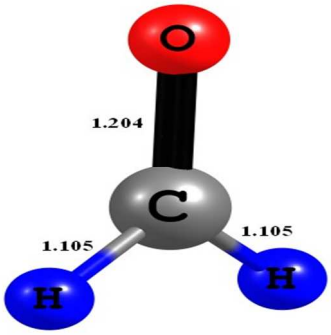

P9, P11

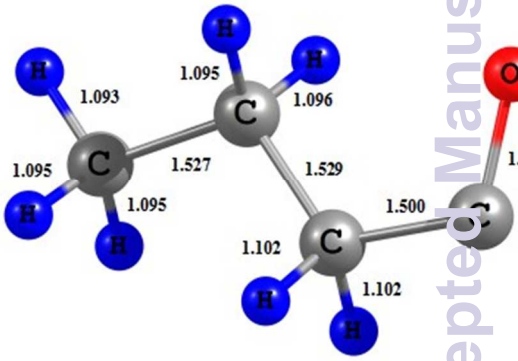

P10

Figure 2. Geometries of the reactant, transition states, and products optimized at the M06-2X/6-31+G(d,p) level of theory. Blue color represents hydrogen and gray color represents carbon, red color represents oxygen in the structures. The bond lengths (Å) given on the structures are obtained at M06-2X/6-31+G(d,p) level of theory.

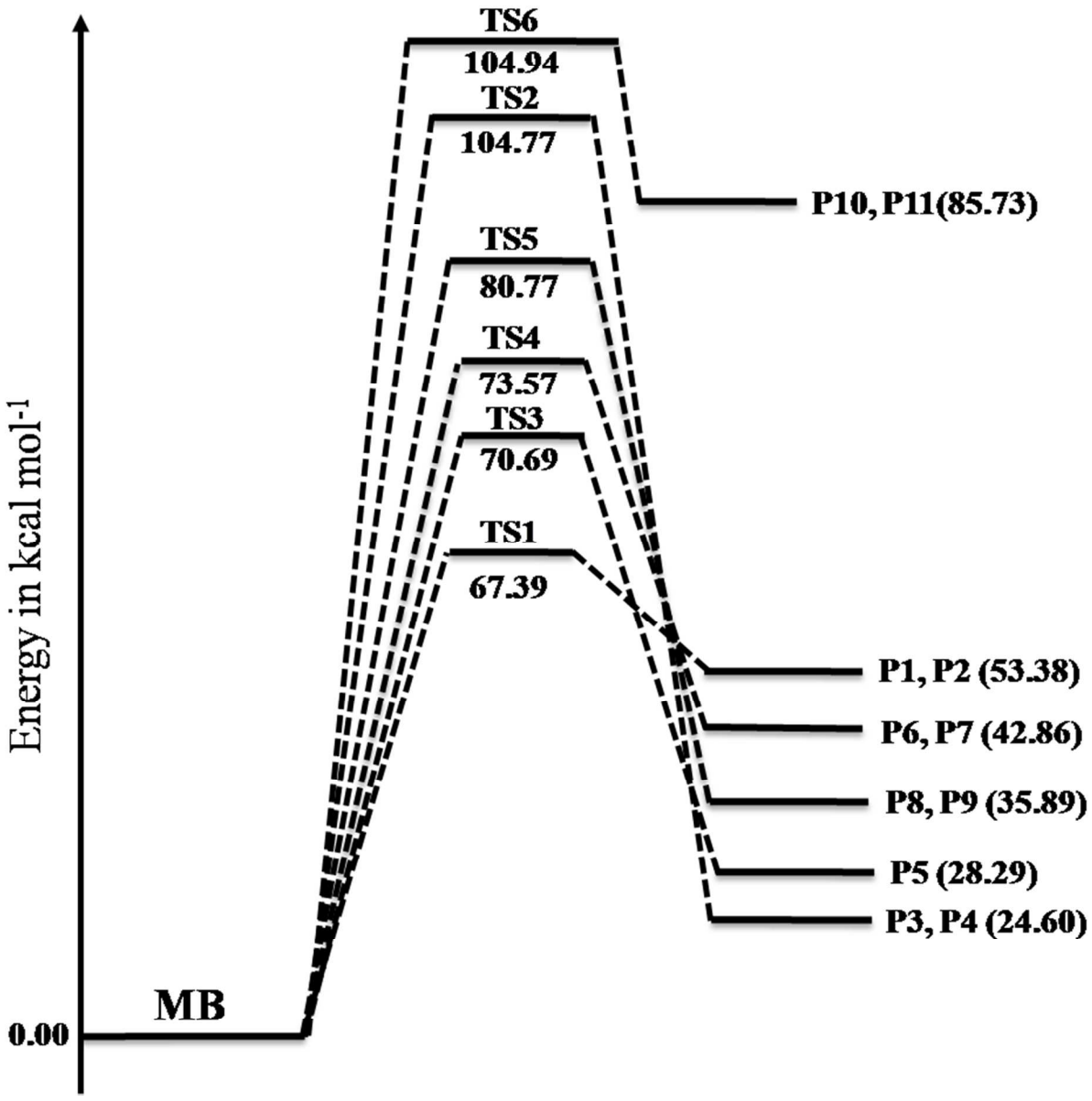

Figure 3. Potential energy surfaces of reaction channels R1-R6 computed using the M06-2X/6-31+G(d,p) level of theory. The energies are given in the units of kcal mol^{-1}.

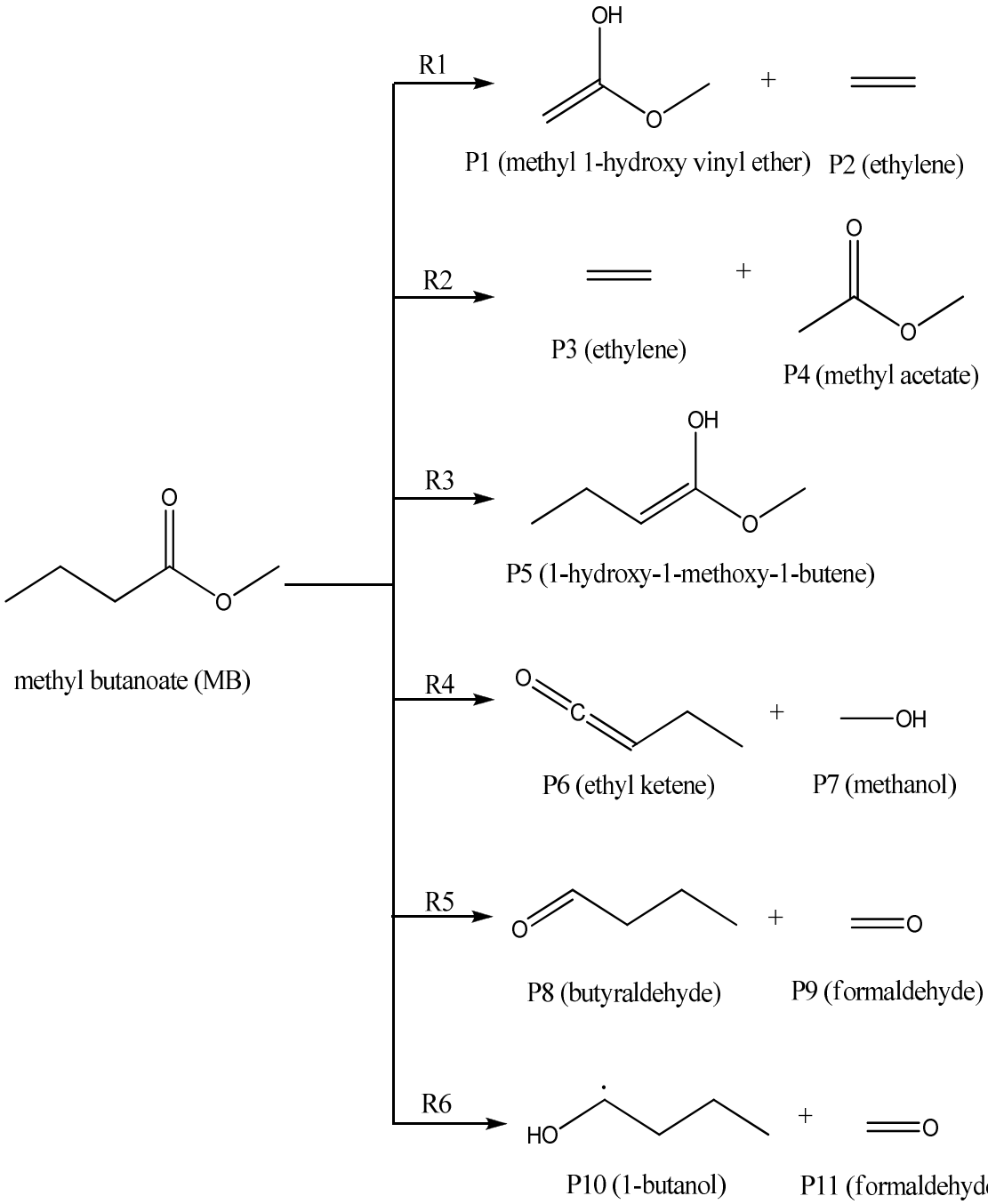

Figure 4. The reaction pathways (R1-R6) for the unimolecular decomposition of methyl butanoate considered in this study.

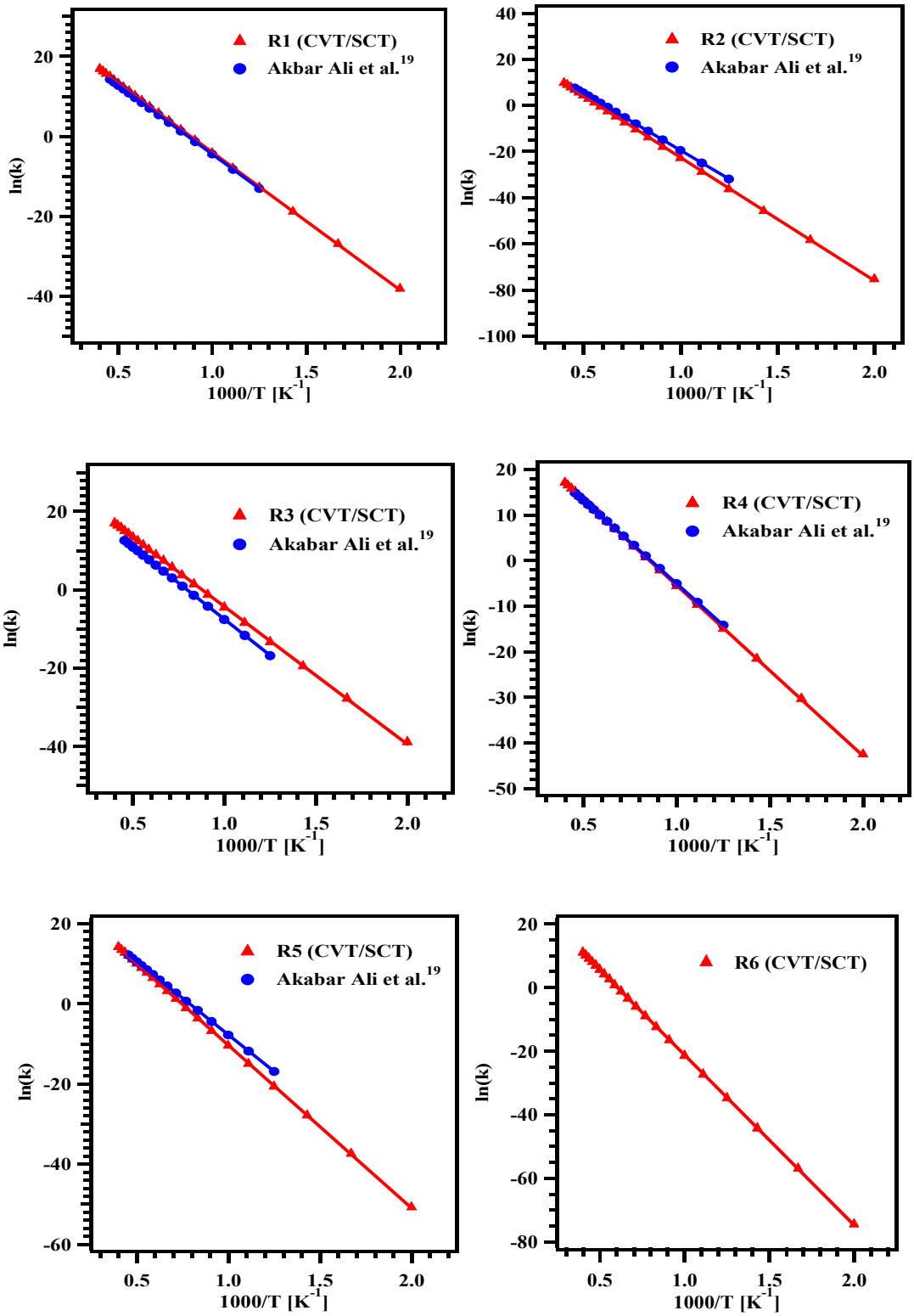

Figure 5. Arrhenius plots for the rate coefficient data obtained for the reaction pathways R1-R6 over the temperature range of 500-2500 K.

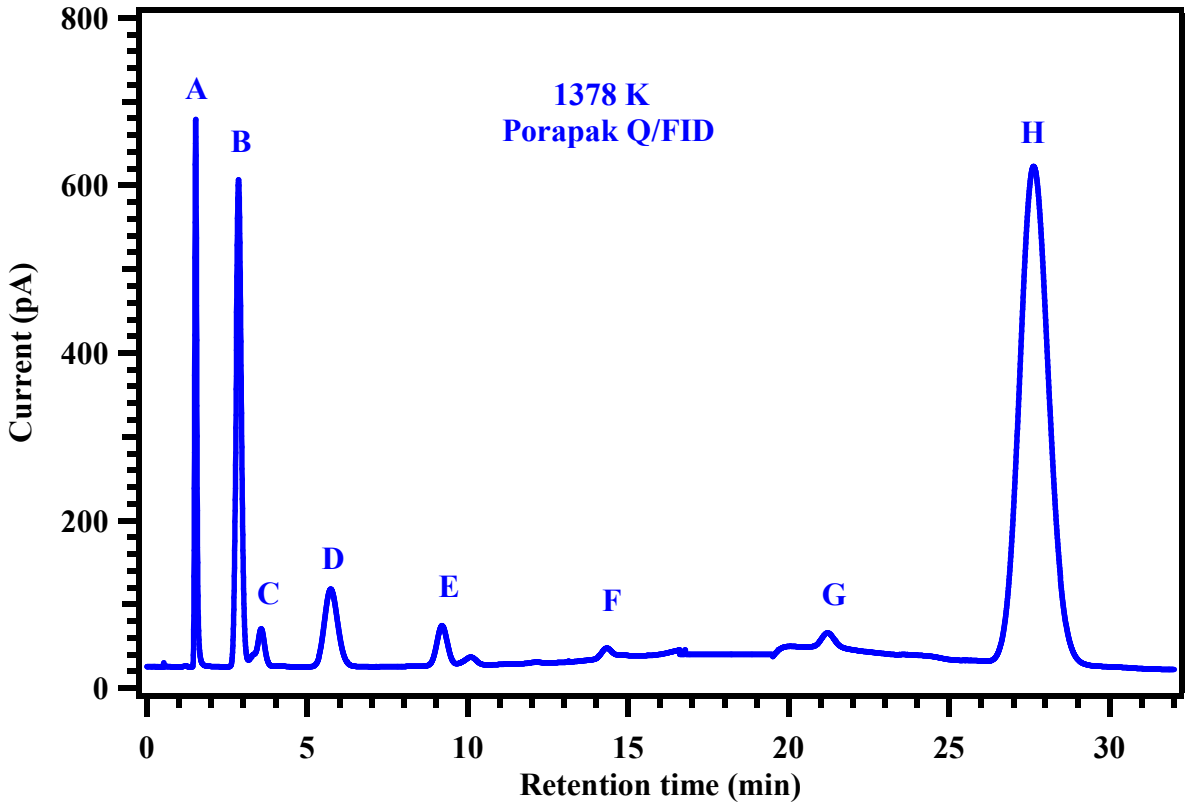

Figure 6. Gas chromatogram showing the products of the post shock mixture of the experiment carried out at 1378 K. The peaks labeled in the chromatogram are A: methane, B: ethylene, C: ethane, D: propylene, E: acetylene, F: 1,3-butadiene, G: methyl acrylate, and H: methyl butanoate.

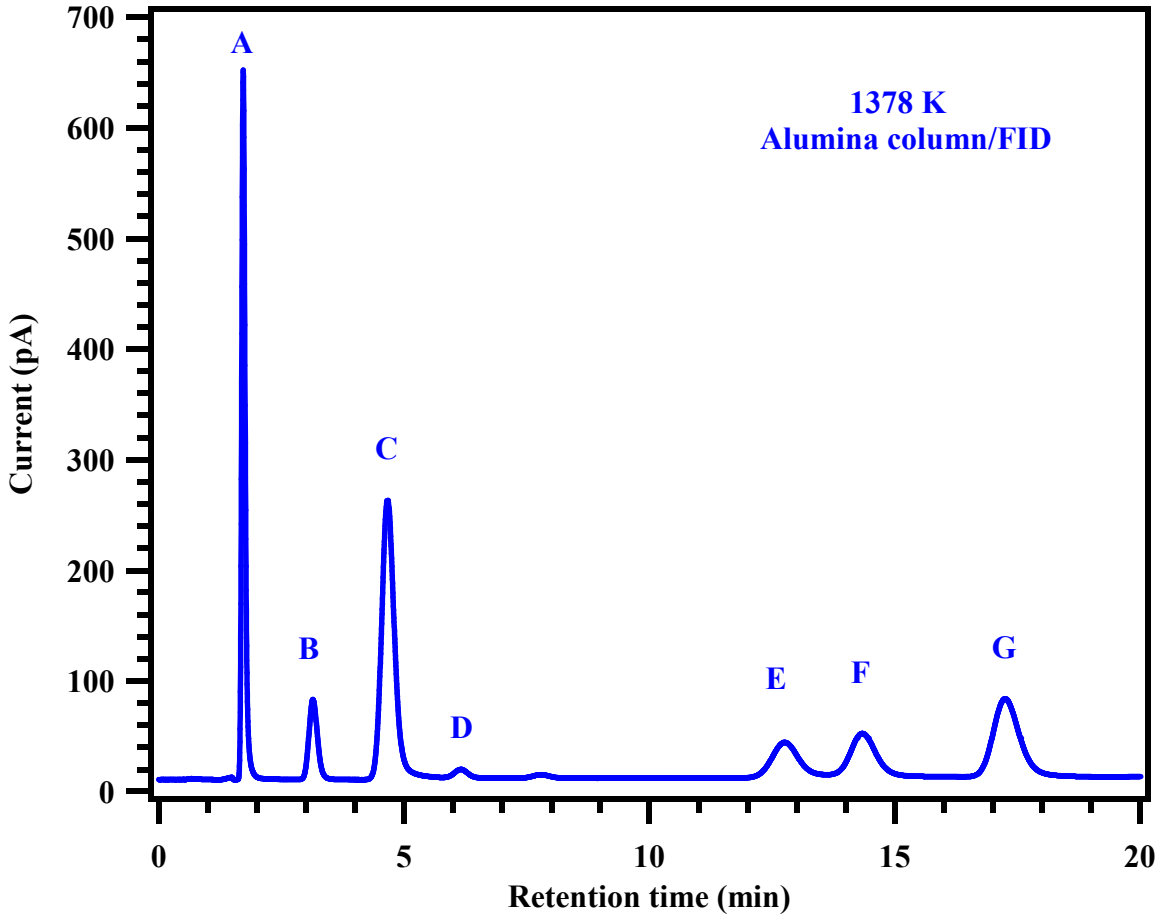

Figure 7. Gas chromatogram showing the products of the post shock mixture of the experiment carried out at 1378 K. The peaks labeled in the chromatogram are (a) methane (b) ethane (c) ethylene (d) 11-DFE (e) acetylene (f) 111-TFE (g) propylene.

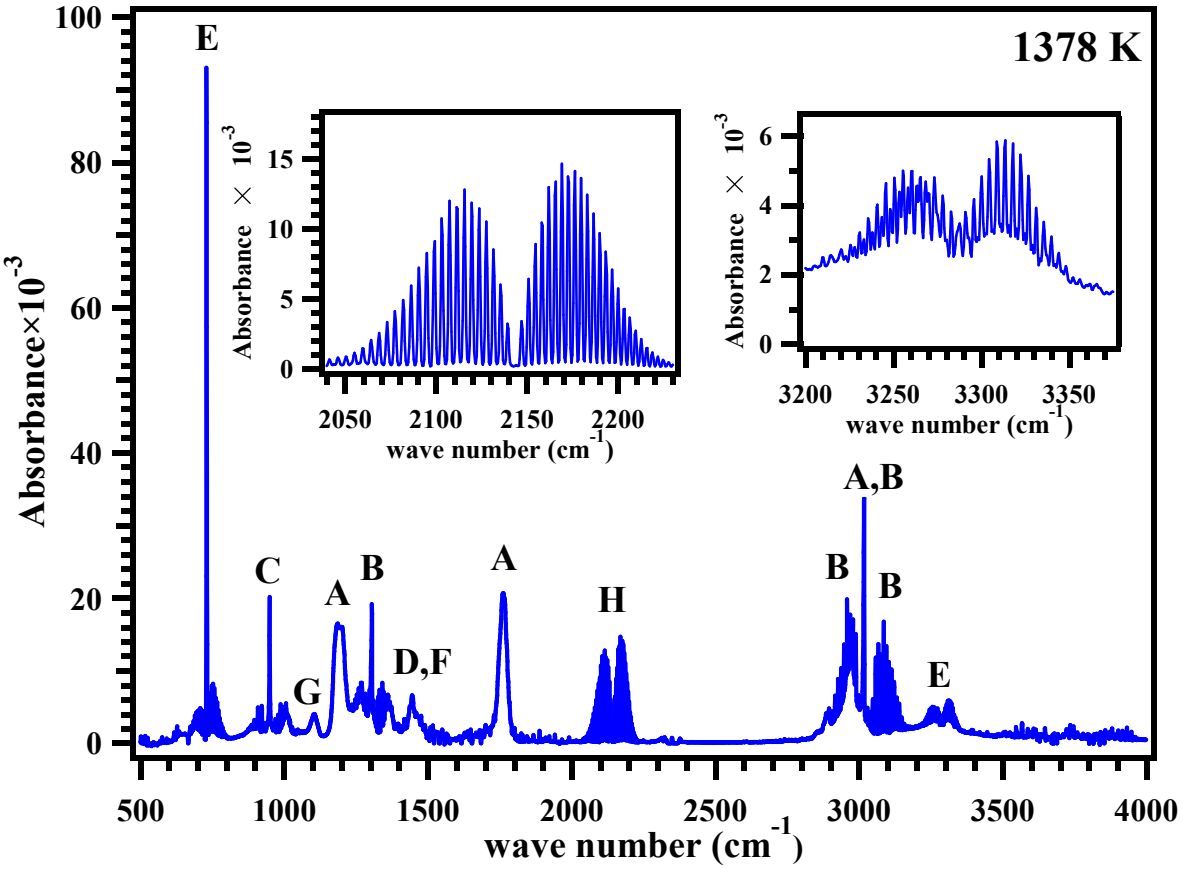

Figure 8. FTIR spectrum of the post shock mixture of methyl butanoate diluted in argon pyrolyzed at 1378 K. All the peaks are assigned to (A) methyl butanoate, (B) methane, (C) ethylene, (D) ethane., (E) acetylene, (F) propylene (G) methyl acrylate (H) CO; Inset plots shown are the expanded regions for CO and acetylene.

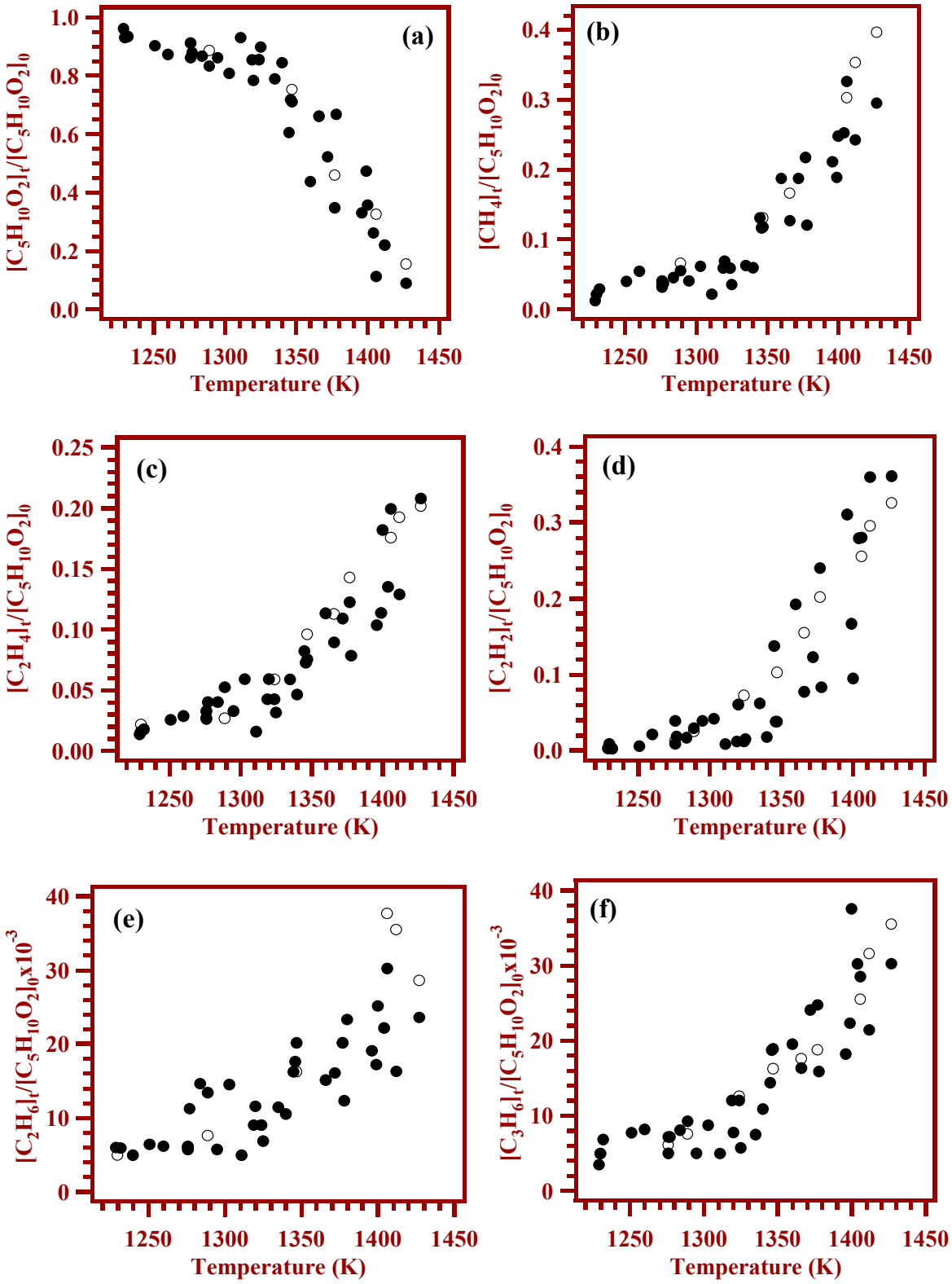

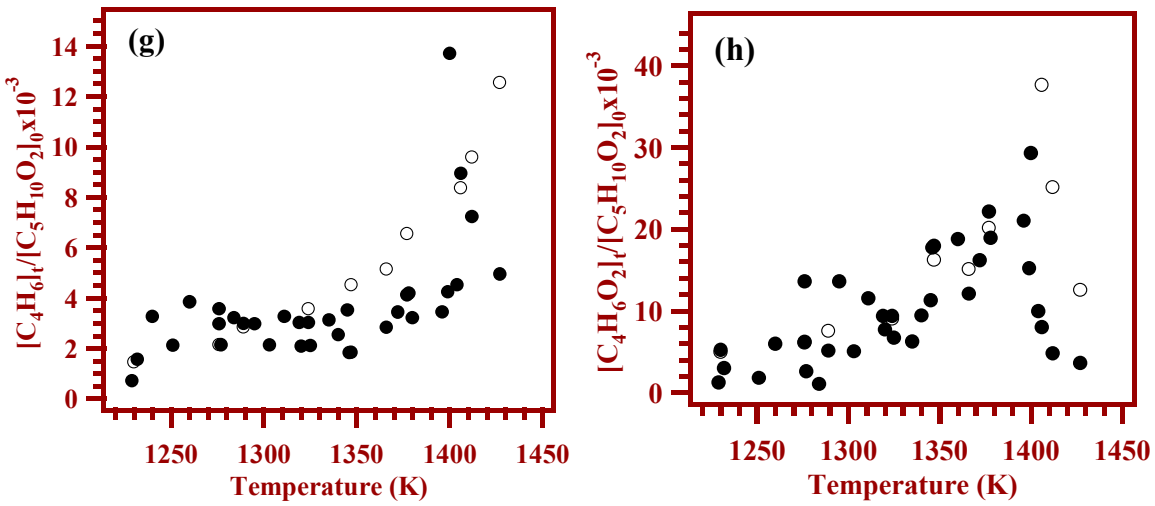

Figure 9. Comparison between the experimentally measured and simulated concentrations of (a) methyl butanoate, (b) methane, (c) ethylene, (d) acetylene, (e) ethane, (f) propylene (g) 1,3-butadiene (h) methyl acrylate. Filled circles on the plot are experimental concentrations and the open circles are simulated concentrations.

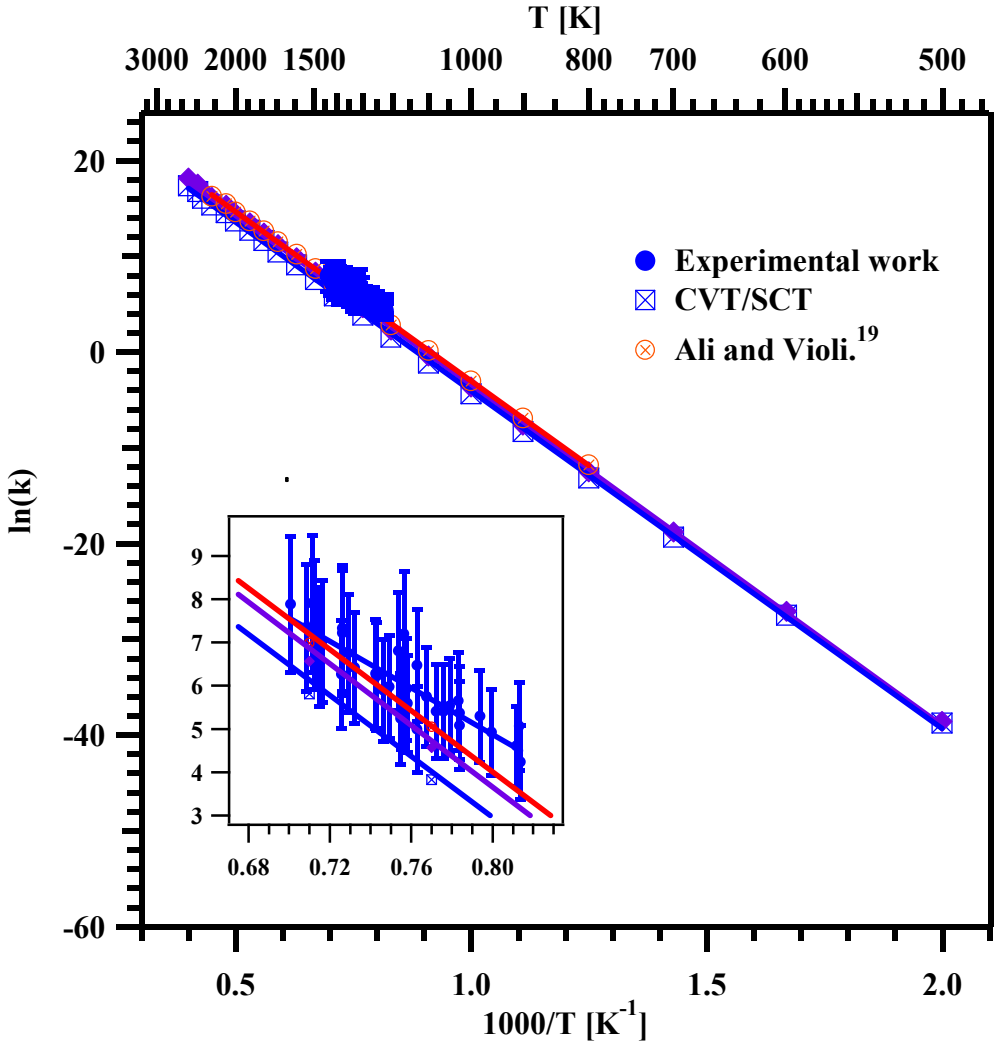

Figure 10. Arrhenius plot for the overall decomposition of methyl butanoate in the temperature range of 1229-1427 K. The obtained temperature dependent rate coefficient for the entire experimental temperature range is k_{total} (1229-1427 K) = (3.08 ± 1.11) × 10^{12} exp (-(53.6 kcal mol^{-1} ± 4.7)/RT) s^{-1}. The insert is the zoom of the data obtained in the present experiments.

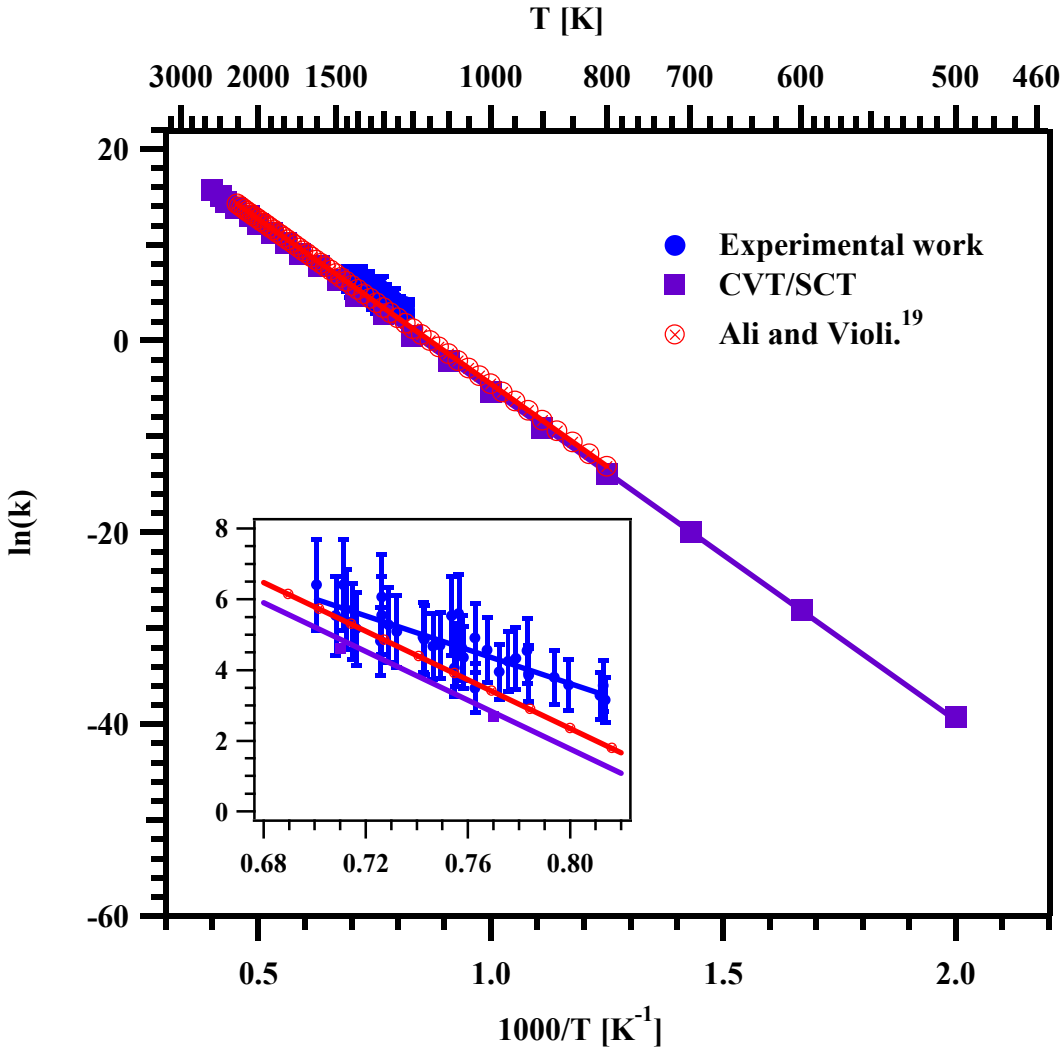

Figure 11. Arrhenius plot for the formation of ethylene in the decomposition of methyl butanoate. The obtained temperature dependent rate coefficient for the entire experimental temperature range is $k_{ethylene}$ (1229-1427 K) = (7.92 ± 2.72) × 10^{9} exp (-(47.6 kcal mol^{-1} ± 4.5)/RT) s^{-1}. The insert is the zoom of the data obtained in the present experiments.

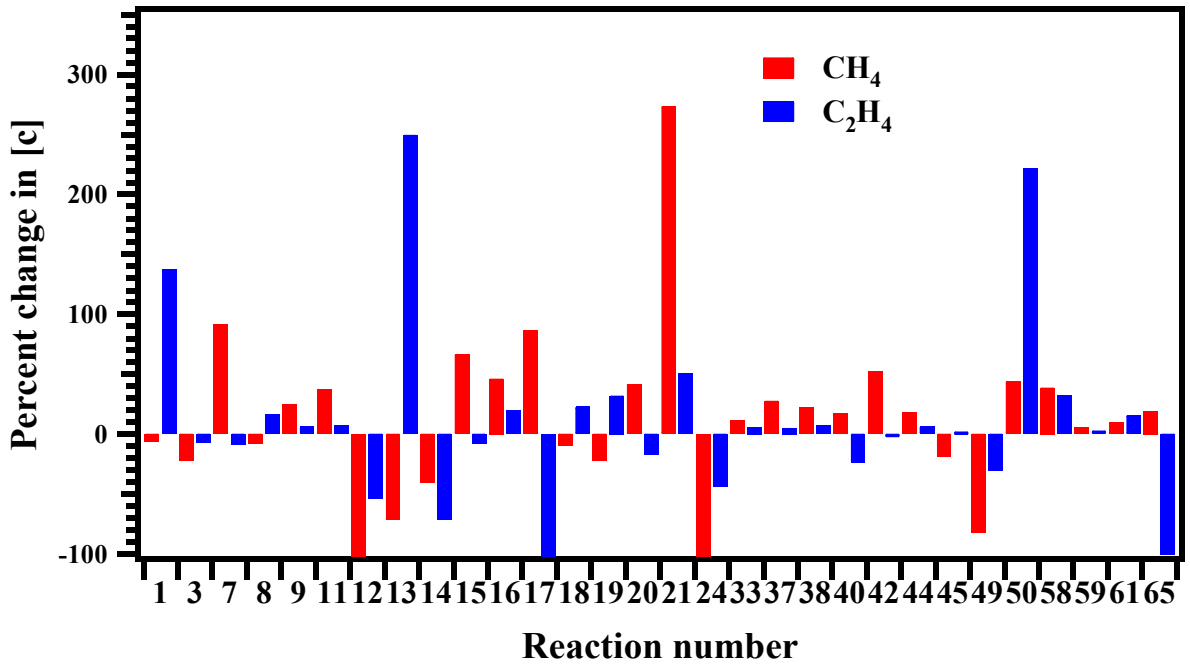

Figure 12. Sensitivity analysis of the proposed reaction scheme carried out at 1347 K for the formation of methane and ethylene.

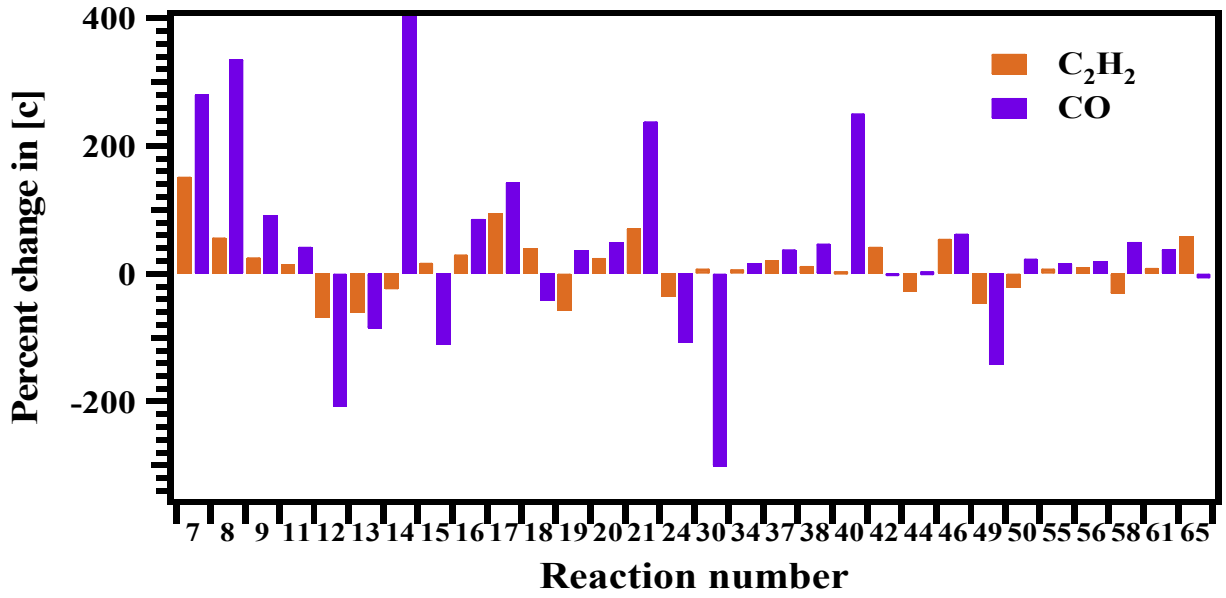

Figure 13. Sensitivity analysis of the proposed reaction scheme carried out at 1347 K for the formation of acetylene and CO.

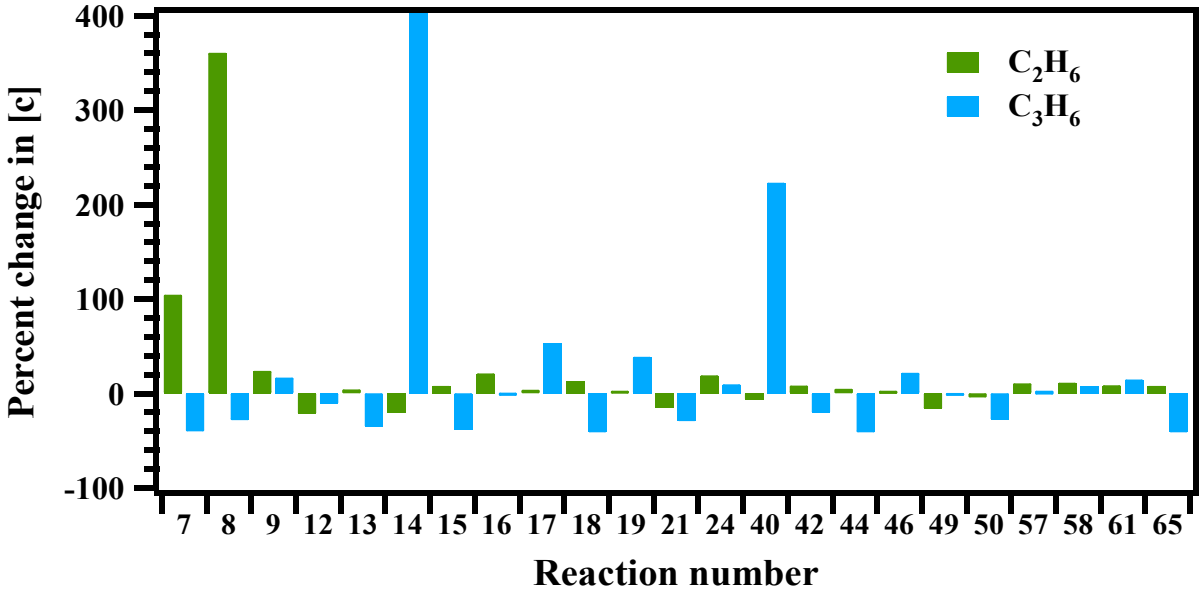

Figure 14. Sensitivity analysis of the proposed reaction scheme carried out at 1347 K for the formation of ethane and propylene.

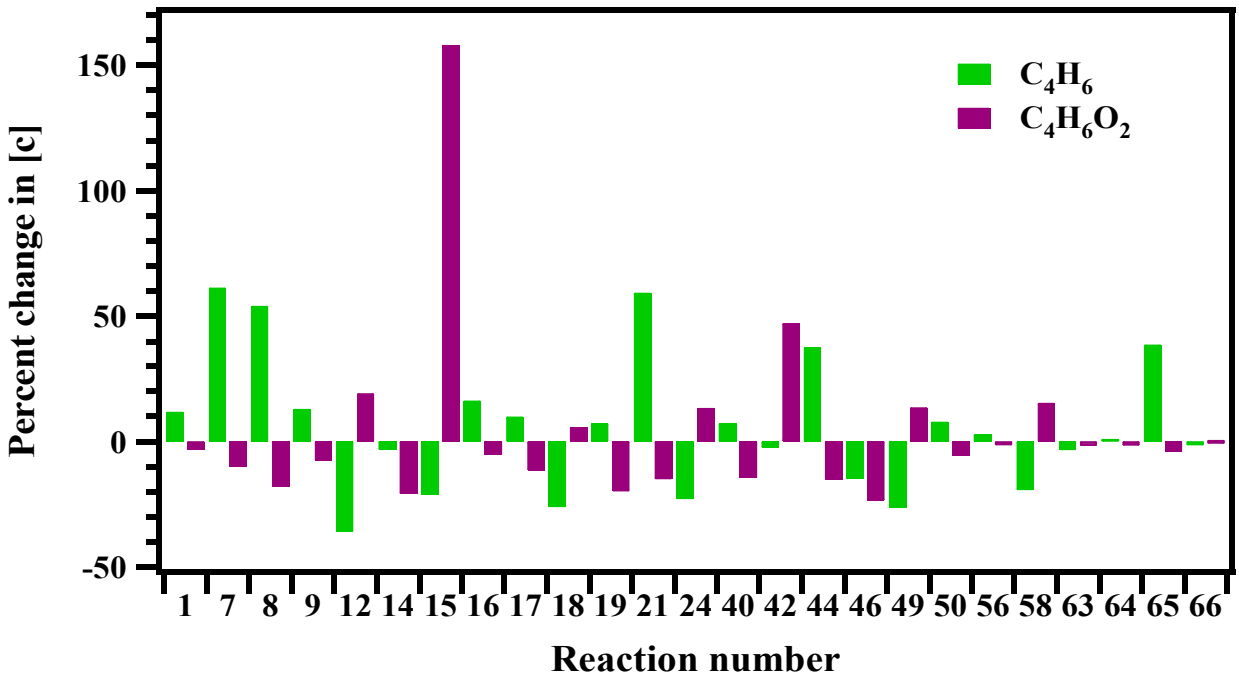

Figure 15. Sensitivity analysis of the proposed reaction scheme carried out at 1347 K for the formation of 1,3-butadiene and methyl acrylate.

Table 1. Energy barriers (kcal mol^{-1}) for thermal decomposition of methyl butanoate reaction via pathways R1-R6, calculated at M06-2X/6-31+G(d,p).

TSs	M06-2X/6-31+G(d,p)
TS1	67.39
TS2	104.76
TS3	70.68
TS4	73.56
TS5	80.77
TS6	104.94

Table 2. The reaction enthalpies ($\Delta H^0_{298\ K}$, kcal mol^{-1}), free energies ($\Delta G^0_{298\ K}$, kcal mol^{-1}) are calculated at M06-2X/6-31+G(d,p) level of theory.

Reaction	ΔH^0 (kcal mol^{-1})	ΔG^0 (kcal mol^{-1})
R1	54.12	43.01
R2	25.47	13.91
R3	28.35	28.26
R4	43.76	31.75
R5	36.66	25.82
R6	86.60	75.48

Table 3. Arrhenius parameters for thermal decomposition of methyl butanoate via reaction pathways (R1-R6) in the temperature range of 500-2500 K.

Pathway	A	Ea (kcal mol^{-1})
R1	$(1.62 \pm 0.22)\times10^{13}$	68.5 ± 0.3
R2	$(2.51 \pm 0.64)\times10^{13}$	106.3 ± 0.5
R3	$(2.66 \pm 0.50)\times10^{13}$	69.9 ± 0.2
R4	$(7.56 \pm 0.98)\times10^{13}$	74.4 ± 0.3
R5	$(1.36 \pm 0.15)\times10^{13}$	80.7 ± 0.2
R6	$(3.51 \pm 0.50)\times10^{13}$	106.4 ± 0.2

Table 4. Experimental conditions and distribution of normalized concentrations of reactant and reaction products in the decomposition of methyl butanoate.

S.No	T5 (K)	Reaction time (**µs**)	$[CH_4]_t/[C_5H_{10}O_2]_0$	$[C_2H_6]_t/[C_5H_{10}O_2]_0$	$[C_2H_4]_t/[C_5H_{10}O_2]_0$	$[C_3H_6]_t/[C_5H_{10}O_2]_0$	$[C_2H_2]_t/[C_5H_{10}O_2]_0$	$[1,3\text{-}C_4H_6]_t/[C_5H_{10}O_2]_0$	$[C_5H_6O_2]_t/[C_5H_{10}O_2]_0$	$[C_5H_{10}O_2]_t/[C_5H_{10}O_2]_0$
1	1229	584	0.01230	0.00596	0.01341	0.003466	0.002673	0.000722	0.001233	0.960237
2	1230	457	0.02156	0.00493	0.01552	0.004954	0.008290	0.003264	0.011533	0.929953
3	1232	682	0.02912	0.00590	0.01750	0.006813	0.002353	0.001567	0.002962	0.933780
4	1240	491	0.02156	0.00493	0.01552	0.004954	0.008290	0.003264	0.011533	0.929953
5	1251	744	0.03984	0.00641	0.02536	0.007734	0.005616	0.011417	0.001778	0.901847
6	1260	684	0.05425	0.00615	0.02847	0.008170	0.021269	0.003841	0.005952	0.871905
7	1276	696	0.04037	0.00566	0.03243	0.004986	0.039022	0.002978	0.013582	0.860962
8	1276	580	0.03148	0.00609	0.02610	0.007164	0.008571	0.003572	0.006210	0.910809
9	1277	452	0.03688	0.01124	0.03998	0.007174	0.018230	0.005439	0.002603	0.878450
10	1284	564	0.04505	0.01462	0.03985	0.008070	0.016793	0.007893	0.001058	0.866678
11	1289	818	0.05498	0.01339	0.05212	0.009239	0.029218	0.002986	0.005118	0.832947
12	1295	670	0.04043	0.00571	0.03243	0.004985	0.039018	0.002978	0.013581	0.860867
13	1303	680	0.06134	0.01450	0.05874	0.008736	0.041740	0.002128	0.005042	0.807775
14	1311	774	0.13060	0.01623	0.08207	0.014363	0.137430	0.003521	0.011278	0.604520
15	1319	588	0.05857	0.00901	0.04229	0.012033	0.011907	0.003025	0.009372	0.853791
16	1320	650	0.06874	0.01155	0.05889	0.007763	0.060447	0.002094	0.007695	0.782825
17	1324	540	0.05871	0.00901	0.04228	0.012031	0.011905	0.003024	0.009370	0.853667
18	1325	570	0.03515	0.00684	0.03139	0.005708	0.014977	0.002114	0.006709	0.897117

19	1327	532	0.15271	0.02345	0.10664	0.027993	0.048701	0.005343	0.017624	0.617540
20	1335	600	0.06247	0.01140	0.05861	0.007483	0.062123	0.003128	0.006242	0.788532
21	1340	467	0.05928	0.01050	0.04617	0.010872	0.017819	0.002544	0.009437	0.843381
22	1346	658	0.11629	0.01760	0.07245	0.018736	0.037860	0.001832	0.017728	0.717498
23	1347	640	0.11775	0.02013	0.07506	0.018871	0.037990	0.001838	0.017932	0.710425
24	1366	670	0.12645	0.01510	0.08925	0.016331	0.077262	0.002844	0.012089	0.660673
25	1372	755	0.18682	0.01608	0.10880	0.024061	0.122621	0.003442	0.016185	0.521997
26	1377	774	0.21688	0.02014	0.12235	0.024747	0.240024	0.006843	0.022138	0.346883
27	1377	674	0.24750	0.03855	0.18181	0.037535	0.094566	0.013705	0.029305	0.357029
28	1378	768	0.12010	0.01231	0.07829	0.015856	0.083282	0.004186	0.018941	0.667027
29	1380	619	0.18679	0.02331	0.11317	0.019489	0.192119	0.008741	0.018788	0.437596
30	1396	970	0.21095	0.01908	0.10338	0.018181	0.310251	0.003449	0.004589	0.330111
31	1399	754	0.18839	0.01719	0.11358	0.022306	0.166663	0.004248	0.015199	0.472420
32	1404	808	0.25211	0.02213	0.13493	0.030202	0.279184	0.009899	0.009944	0.261597
33	1406	804	0.32549	0.03765	0.19912	0.028518	0.279981	0.008944	0.007975	0.112323
34	1412	978	0.24215	0.01627	0.12876	0.021409	0.359627	0.007228	0.004809	0.219753
35	1427	908	0.29436	0.02359	0.20773	0.015344	0.360894	0.004949	0.003619	0.089506

Table 5. Proposed reaction scheme for the decomposition of methyl butanoate with 39 reaction species and 66 elementary reactions.[a]

S.No	Reaction	A	n	E_a	Reference
R1	MB → C_2H_4 + CH_2=C(OH)-O-CH_3	1.62×10^{13}	0.00	68.46	This work
R2	MB → CH_3-C(O)-O-CH_3 + C_2H_4	2.51×10^{13}	0.00	106.30	This work
R3	MB → CH_3-CH_2-CH=C(OH)-O-CH_3	2.66×10^{13}	0.00	69.98	This work
R4	MB → CH_3-CH_2-CH=C(OH)-O-CH_3 + CH_3-OH	7.56×10^{13}	0.00	74.36	This work
R5	MB → CH_3-CH_2-CH_2-C(O)-H + H-C(O)-H	1.36×10^{13}	0.00	80.71	This work
R6	MB → CH_3-CH_2-CH_2-C(OH) + H-C(O)-H	1.03×10^{14}	0.00	106.38	This work
R7	MB → $CH_3^{\bullet}$ + $CH_2^{\bullet}$-CH_2-C(O)-O-CH_3	5.41×10^{15}	-0.19	80.00	19
R8	MB → CH_3-$CH_2^{\bullet}$ + $CH_2^{\bullet}$-C(O)-O-CH_3	4.03×10^{15}	-0.18	77.70	19
R9	MB → CH_3-CH_2- $CH_2^{\bullet}$ + CH_3-O-C(O)$^{\bullet}$	2.15×10^{16}	-0.25	87.60	19
R10	MB → CH_3-CH_2-CH_2-C(O)$^{\bullet}$ + CH_3-O$^{\bullet}$	4.30×10^{15}	-0.28	92.50	19
R11	MB → CH_3-CH_2-CH_2-C(O)-O$^{\bullet}$ + $CH_3^{\bullet}$	6.58×10^{15}	-0.22	83.60	19
R12	MB + H → CH_3-CH_2-CH_2-C(O)-O-$CH_2^{\bullet}$ + H_2	9.61×10^{2}	3.34	3.94	42
R13	MB + H → $CH_2^{\bullet}$-CH_2-CH_2-C(O)-O-CH_3 + H_2	1.50×10^{4}	2.96	4.29	42
R14	MB + H → CH_3-$CH^{\bullet}$-CH_2-C(O)-O-CH_3 + H_2	4.95×10^{5}	2.47	3.26	42
R15	MB + H → CH_3-CH_2-$CH^{\bullet}$-C(O)-O-CH_3 + H_2	3.18×10^{4}	2.77	2.28	42
R16	CH_3-CH_2-CH_2-C(O)-O-$CH_2^{\bullet}$ + H_2 → MB + H	2.87×10^{3}	2.68	11.01	42
R17	$CH_2^{\bullet}$-CH_2-CH_2-C(O)-O-CH_3 + H_2 → MB + H	2.22×10^{1}	3.26	9.06	42
R18	CH_3-$CH^{\bullet}$-CH_2-C(O)-O-CH_3 + H_2 → MB + H	3.38×10^{2}	2.83	11.41	42
R19	CH_3-CH_2-$CH^{\bullet}$-C(O)-O-CH_3 + H_2 → MB + H	4.71×10^{1}	3.28	14.92	42

R20	MB + $CH_3^{\bullet}$ → CH_3-CH_2-CH_2-C(O)-O-$CH_2^{\bullet}$ + CH_4	2.28×10^{-8}	5.88	6.79	42
R21	MB + $CH_3^{\bullet}$ → $CH_2^{\bullet}$-CH_2-CH_2-C(O)-O-CH_3 + CH_4	1.50×10^{4}	2.96	4.29	42
R22	MB + $CH_3^{\bullet}$ → CH_3-$CH^{\bullet}$-CH_2-C(O)-O-CH_3 + CH_4	1.44×10^{-5}	4.97	7.18	42
R23	MB + $CH_3^{\bullet}$ → CH_3-CH_2-$CH^{\bullet}$-C(O)-O-CH_3 + CH_4	1.87×10^{-5}	4.97	6.06	42
R24	$CH_2^{\bullet}$-CH_2-CH_2-C(O)-O-CH_3 + CH_4 → MB + $CH_3^{\bullet}$	2.22×10^{1}	3.26	9.06	42
R25	CH_3-$CH^{\bullet}$-CH_2-C(O)-O-CH_3 + CH_4 → MB + $CH_3^{\bullet}$	4.35×10^{-8}	5.59	13.85	42
R26	CH_3-CH_2-$CH^{\bullet}$-C(O)-O-CH_3 + CH_4 → MB + $CH_3^{\bullet}$	1.24×10^{-7}	5.71	17.24	42
R27	CH_3-CH_2-CH_2-C(O)-O-$CH_2^{\bullet}$ + CH_4 → MB + $CH_3^{\bullet}$	3.02×10^{-7}	5.48	12.39	42
R28	$CH_2^{\bullet}$-CH_2-CH_2-C(O)-O-CH_3 → CH_3-CH_2-CH_2-C(O)-O-$CH_2^{\bullet}$	1.34×10^{-8}	5.43	15.75	42
R29	$CH_2^{\bullet}$-CH_2-CH_2-C(O)-O-CH_3 → CH_3-CH_2-$CH^{\bullet}$-C(O)-O-CH_3	1.49×10^{-23}	10.03	16.71	42
R30	$CH_2^{\bullet}$-CH_2-CH_2-C(O)-O-CH_3 → CH_3-$CH^{\bullet}$-CH_2-C(O)-O-CH_3	5.08×10^{-17}	8.45	23.69	42
R31	CH_3-$CH^{\bullet}$-CH_2-C(O)-O-CH_3 → $CH_2^{\bullet}$-CH_2-CH_2-C(O)-O-CH_3	1.05×10^{-17}	8.50	26.79	42
R32	CH_3-$CH^{\bullet}$-CH_2-C(O)-O-CH_3 → CH_3-CH_2-$CH^{\bullet}$-C(O)-O-CH_3	9.71×10^{-9}	5.71	23.82	42
R33	CH_3-$CH^{\bullet}$-CH_2-C(O)-O-CH_3 → CH_3-CH_2-CH_2-C(O)-O-$CH_2^{\bullet}$	1.43×10^{-7}	5.16	16.82	42
R34	CH_3-CH_2-$CH^{\bullet}$-C(O)-O-CH_3 → $CH_2^{\bullet}$-CH_2-CH_2-C(O)-O-CH_3	1.33×10^{-23}	10.29	24.58	42
R35	CH_3-CH_2-$CH^{\bullet}$-C(O)-O-CH_3 → CH_3-$CH^{\bullet}$-CH_2-C(O)-O-CH_3	4.83×10^{-8}	5.92	28.60	42
R36	CH_3-CH_2-$CH^{\bullet}$-C(O)-O-CH_3 → CH_3-CH_2-CH_2-C(O)-O-$CH_2^{\bullet}$	9.80×10^{-11}	6.55	21.75	42
R37	CH_3-CH_2-CH_2-C(O)-O-$CH_2^{\bullet}$ → CH_3-CH_2-$CH^{\bullet}$-C(O)-O-CH_3	6.62×10^{-10}	6.26	15.65	42
R38	CH_3-CH_2-CH_2-C(O)-O-$CH_2^{\bullet}$ → CH_3-$CH^{\bullet}$-CH_2-C(O)-O-CH_3	2.40×10^{-6}	5.07	15.48	42
R39	CH_3-CH_2-CH_2-C(O)-O-$CH_2^{\bullet}$ → $CH_2^{\bullet}$-CH_2-CH_2-C(O)-O-CH_3	4.06×10^{-8}	5.40	17.51	42
R40	CH_3-$CH^{\bullet}$-CH_2-C(O)-O-CH_3 → C_3H_6 + C(O)$^{\bullet}$-O-CH_3	4.53×10^{12}	0.33	34.27	42
R41	CH_3-CH_2-$CH^{\bullet}$-C(O)-O-CH_3 → $CH_3O^{\bullet}$ + CH_3-CH_2-CH=C=O	1.46×10^{12}	0.61	53.28	42

R42	CH_3-CH_2-$CH^{\bullet}$-C(O)-O-CH_3 → CH_2=CH-C(O)-O-CH_3 + $^{\bullet}CH_3$	1.33×10^{11}	0.97	34.88	42
R43	$CH_2^{\bullet}$-CH_2-C(O)-O-CH_3 → CH_2=CH-C(O)-O-CH_3 + H	1.53×10^{8}	1.57	38.38	42
R44	CH_2=CH-C(O)-O-CH_3 + H → CH_2=CH-C(O)-O-$CH_2^{\bullet}$ + H_2	1.42×10^{3}	3.29	3.98	42
R45	CH_2=CH-C(O)-O-CH_3 + H → $CH_2^{\bullet}$-CH_2-C(O)-O-CH_3	4.18×10^{8}	1.56	1.70	42
R46	CH_2=CH-C(O)-O-CH_3 + H → CH=CH-C(O)-O-CH_3 + H_2	2.80×10^{6}	2.36	12.21	42
R47	CH_2=CH-C(O)-O-CH_3 + H → CH_2=$C^{\bullet}$-C(O)-O-CH_3 + H_2	1.98×10^{7}	2.05	12.16	42
R48	$CH^{\bullet}$=CH-C(O)-O-CH_3 → C_2H_2 + C(O)$^{\bullet}$-O-CH_3	5.76×10^{12}	0.82	38.50	42
R49	CH_3-CH_2-CH_2-C(O)-O-$CH_2^{\bullet}$ → CH_3-CH_2-CH_2-C(O)$^{\bullet}$ + HC(O)H	1.23×10^{13}	0.38	36.71	42
R50	CH_2-CH_2-CH_2-C(O)-O-CH_3 → C_2H_4 + $CH_2^{\bullet}$-C(O)-O-CH_3	5.25×10^{11}	0.50	26.59	42
R51	CH_2=CH-C(O)-O-$CH_2^{\bullet}$ → $CH_2^{\bullet}$-CH=CO + H-C(O)-H	2.83×10^{11}	0.49	30.00	42
R52	CH_2-CH=CO → $C_2H_3^{\bullet}$ + CO	3.47×10^{12}	0.63	27.21	42
R53	CH_3-CH_2-$CH_2^{\bullet}$ → C_3H_6 + H	4.14×10^{12}	0.17	35.62	43
R54	2 $CH_3^{\bullet}$ → C_2H_6	6.80×10^{14}	-0.60	0.00	44
R55	2 $CH_3^{\bullet}$ → C_2H_4 + H_2	9.90×10^{15}	0.00	32.98	45
R56	2 $CH_3^{\bullet}$ → $C_2H_5^{\bullet}$ + H	2.41×10^{13}	0.00	12.87	46
R57	CH_3-O-C(O)-$CH_2^{\bullet}$ → CH_2=C(O) + $CH_3O^{\bullet}$	1.28×10^{12}	0.66	49.26	42
R58	CH_2=C(O) + H → CO + $CH_3^{\bullet}$	7.77×10^{8}	1.45	2.78	47
R59	CH_3-O-C(O)$^{\bullet}$ → CO + CH_3-$O^{\bullet}$	8.02×10^{11}	0.65	21.12	42
R60	CH_3-$O^{\bullet}$ → H-C(O)-H + H	1.87×10^{25}	-3.00	24.31	48
R61	H-C(O)-H + H → CH_3-$O^{\bullet}$	1.99×10^{8}	1.66	1.72	42
R62	C_3H_6 + $C_2H_3^{\bullet}$ → C_4H_6 + CH_3	7.23×10^{11}	0.00	5.01	49
R63	$C_2H_3^{\bullet}$ → C_2H_2 + H	2.00×10^{14}	0.00	39.74	50

R64	$CH_4 + C_3H_5^{\bullet} \rightarrow C_3H_6 + CH_3^{\bullet}$	3.99×10^{1}	3.40	23.25	49
R65	$C_2H_4 + H \rightarrow C_2H_3^{\bullet} + H_2$	5.24×10^{14}	0.00	14.90	50
R66	$C_3H_6 + C_2H_5^{\bullet} \rightarrow C_2H_6 + C_3H_5^{\bullet}$	2.23	3.50	6.64	49

[a]Rate expressions are given in the form of $k = A \exp(-E_a/RT)$ and $k = AT^n \exp(-E_a/RT)$. The units of the rate coefficients are s^{-1} and $cm^3mol^{-1}s^{-1}$ for first and second order reactions respectively. The units for the activation barrier are kcal mol^{-1}.

Table 6. The present experimental and theoretical rate parameters for total decomposition of methyl butanoate and formation of ethylene in the studied temperature range.

Total decomposition of MB			
Temperature range	A (s^{-1})	E_a (kcal mol^{-1})	Reference
1229-1427 K	$(3.08 \pm 1.11) \times 10^{12}$	53.6 ± 4.7	This work (experiment)
500-2500 K	$(9.05 \pm 1.91) \times 10^{13}$	70.7 ± 2.0	This work (CVT/SCT)
Ethylene formation from decomposition of MB			
1229-1427 K	$(7.92 \pm 2.72) \times 10^{9}$	47.6 ± 4.5	This work (experiment)
500-2500 K	$(5.52 \pm 0.89) \times 10^{12}$	68.5 ± 1.6	This work (CVT/SCT)

Table of contents: (TOC)

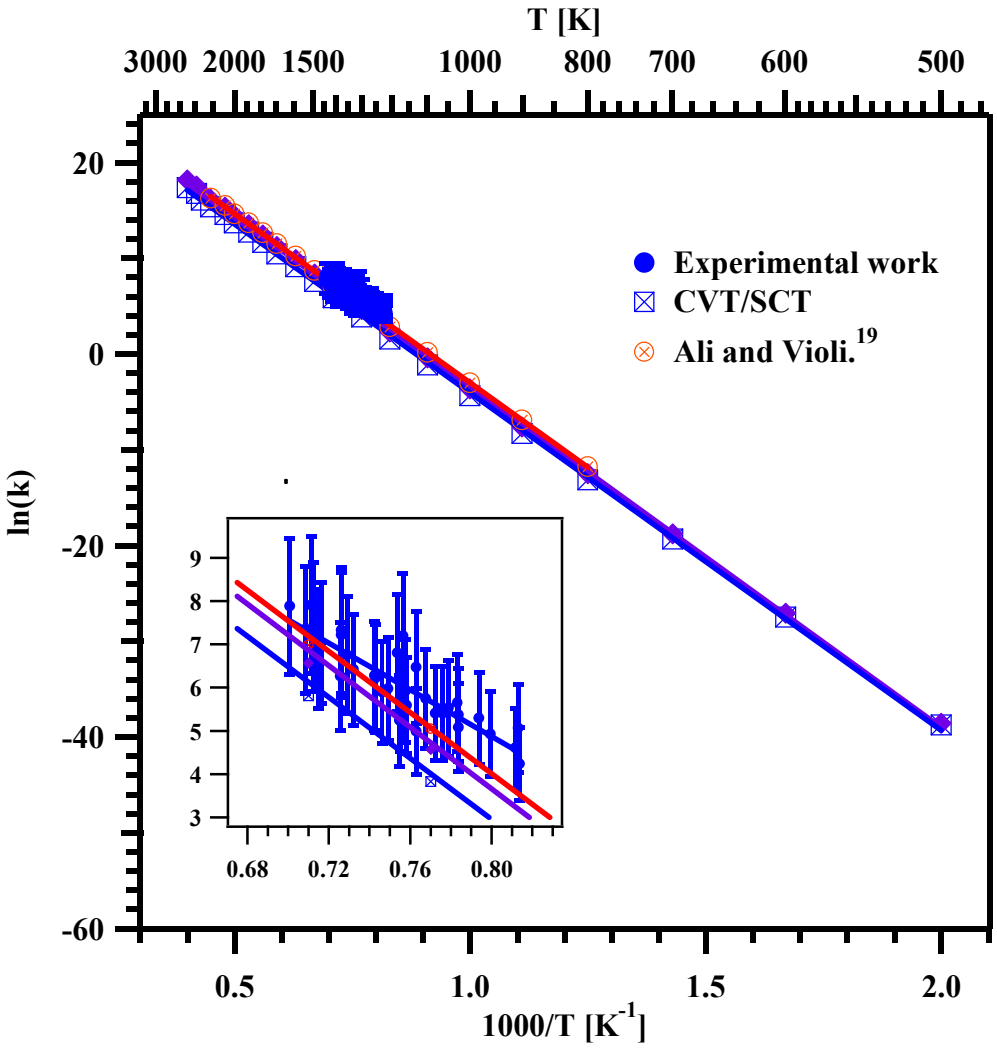

The rate coefficients for total decomposition of MB in the temperature range of 1229 – 1427 K, were reported.